The Neutrino Factory: Update of the Status of the Research and Development

(The Neutrino Factory and Muon Collider Collaboration)

C. Albright,[1] V. Barger,[2] A. Blondel,[3] S.A. Bogacz,[4] S. Brice,[1] S. Caspi,[5]
J. Cobb,[6] S. Geer,[1] J.J. Gomez-Cadenas,[7] M. Goodman,[8] D. Harris,[1]
P. Huber,[9] A. Jansson,[1] T. Kobilarcik,[1] M. Lindner,[9] O. Mena,[1]
P. Rapidis,[1] K. Whisnant,[10] W. Winter,[9] H. Witte,[6] and M. Zisman[5]

[1]*Fermi National Accelerator Laboratory, Batavia, IL 60510, USA*
[2]*Dept. of Physics, University of Wisconsin, Madison, WI 53706, USA*
[3]*DPNC, Section de Physique, Université de Genève, Switzerland*
[4]*Jefferson Laboratory, 12000 Jefferson Avenue, Newport News, VA 23606, USA*
[5]*Lawrence Berkeley National Laboratory, Berkeley, CA 94720, USA*
[6]*Oxford University, Oxford OX1 3RH, UK*
[7]*Departamento de Física Teórica and IFIC,*
Universidad de Valencia, E-46100 Burjassot, Spain
[8]*Argonne National Laboratory, Argonne, IL 60439, USA*
[9]*Technischen Universität München, Garching, Germany*
[10]*Iowa State University, Ames, IA 50011, USA*

(Dated: March 21, 2005)

Abstract

The long-term prospects for fully exploring three-flavor mixing in the neutrino sector depend upon an ongoing and increased investment in the appropriate accelerator R&D. One of the concepts with significant potential, is the Neutrino Factory. This facility would dramatically improve our ability to test the three-flavor mixing framework, measure *CP* violation in the lepton sector, and perhaps determine the neutrino mass hierarchy, and, if necessary, probe extremely small values of the mixing angle θ_{13}. The sensitivity that could be achieved is described in details.

A Neutrino Factory could not be built without significant and sustained R&D. This effort has been ongoing in the U.S., Europe and Japan over the last few years and significant progress has been made towards optimizing the design, developing and testing the required accelerator components, and significantly reducing the cost.

The recent progress reported in this article, was spurred by the year-long Study on the Physics of Neutrinos organized by the APS Divisions of Particles and Fields and of Nuclear Physics, together with the APS Divisions of Astrophysics and the Physics of Beams [1].

I. INTRODUCTION

A Neutrino Factory [2, 3, 4] facility offers an exciting options for the long-term neutrino physics program. In the U.S. there has been a significant investment in developing the concepts and technologies required for such a accelerator complex.

New accelerator technologies offer the possibility of building, in the not-too-distant future, an accelerator complex to produce and capture more than 10^{20} muons per year [3]. It has been proposed to build a Neutrino Factory by accelerating the muons from this intense source to energies of several tens of GeV, injecting them into a storage ring having long straight sections, and exploiting the intense neutrino beams that are produced by muons decaying in the straight sections. The decays

$$\mu^- \to e^- \nu_\mu \bar{\nu}_e \ , \qquad \mu^+ \to e^+ \bar{\nu}_\mu \nu_e \tag{1}$$

offer exciting possibilities to pursue the study of neutrino oscillations and neutrino interactions with exquisite precision.

To realize such intense muon source, a Neutrino Factory requires an intense multi-GeV proton source capable of producing a primary proton beam with a beam power of 1–2 MW or more on target. This is just the proton source required in the medium term for Neutrino Superbeams; hence, there is a natural evolution from Superbeam experiments to Neutrino Factory experiments in the longer term.

The physics case for a Neutrino Factory will depend upon results from the next round of planned neutrino oscillation experiments. If the unknown mixing angle θ_{13} is small, such that $\sin^2 2\theta_{13} < O(10^{-2})$, or if there is a surprise and three-flavor mixing does not completely describe the observed phenomenology, then answers to some or all of the most important neutrino oscillation questions will require a Neutrino Factory. If $\sin^2 2\theta_{13}$ is large, just below the present upper limit, and if there are no experimental surprises, the physics case for a Neutrino Factory will depend on the values of the oscillation parameters, the achievable sensitivity that will be demonstrated by the first generation of ν_e appearance experiments, and the nature of the second generation of basic physics questions that will emerge from the first round of results. In either case (large or small θ_{13}), in about a decade the neutrino community may need to insert a Neutrino Factory into the global neutrino plan. The option to do this in the next 10 years will depend upon the accelerator R&D that is done during the intervening period.

In the U.S., the *Neutrino Factory and Muon Collider Collaboration* (referred to herein as the Muon Collaboration, or MC) [5] is a collaboration of 130 scientists and engineers engaged in carrying out the accelerator R&D that is needed before a Neutrino Factory could be inserted into the global plan. Much technical progress has been made over the last few years, and the required key accelerator experiments are now in the process of being proposed and approved. In addition to the U.S. effort, there are active Neutrino Factory R&D groups in Europe [6], [7] and Japan [8], and much of the R&D is performed and organized as an international endeavor. Thus, because a Neutrino Factory is potentially the key facility for the long-term neutrino program, Neutrino Factory R&D is an important part of the *present* global neutrino program. Indeed, the key R&D experiments are seeking funding now, and will need to be supported if Neutrino Factories are to be an option for the future.

In this report, we summarize the expected sensitivities of Neutrino Factory neutrino oscillation experiments, and the status of the R&D. We describe an updated Neutrino Factory design that demonstrates significant progress toward cost reduction for this ambitious facility. The report is organized as follows. Section II describes in some detail the Neutrino Factory design concept. In Section III, Neutrino Factory beam property is described and compared with conventional neutrino beams. The neutrino oscillation physics reach is presented in Section IV. Progress on Neutrino Factory design is discussed in Section V. The Neutrino Factory R&D programs is described in Section VI. A summary is given in Section VII.

II. MACHINE CONCEPT

In this Section we describe the basic machine concepts that are used to create a Neutrino Factory facility. This facility is a *secondary beam* machine, that is, a production beam is used to create the secondary beam that eventually provides the neutrino flux for the detector.

For a Neutrino Factory, the production beam is a high intensity proton beam of moderate energy (beams of 2–50 GeV have been considered by various groups [9, 10]) that impinges on a target, typically a high-Z material (e.g. Hg). The collisions between the proton beam and the target nuclei produce a secondary pion beam that quickly decays (26.0 ns) into a longer-lived (2.2 μs) muon beam. The remainder of the Neutrino Factory is used to condition the muon beam (see Section V), accelerate it rapidly to the desired final energy of a few

tens of GeV, and store it in a decay ring having a long straight section oriented such that decay neutrinos produced there will hit a detector located thousands of kilometers from the source.

The various components of a Neutrino Factory, based in part on the most recent Feasibility Study (Study-II, referred to herein as FS2) [9] that was carried out jointly by BNL and the U.S. *Neutrino Factory and Muon Collider Collaboration*, are described briefly below. Details of the design discussed here are based on the specific scenario of sending a neutrino beam from BNL to a detector in Carlsbad, New Mexico. More generally, however, the design exemplifies a Neutrino Factory for which two Feasibility Studies [9, 10] have demonstrated technical feasibility (provided the challenging component specifications are met), established a cost baseline, and established the expected range of physics performance. It is worth noting that the Neutrino Factory design we envision could fit comfortably on the site of an existing laboratory, such as BNL or FNAL. As part of the current Study, we have developed improved methods for accomplishing some of the needed beam manipulations. These improvements are included in the description below.

The main ingredients of a Neutrino Factory include:

- **Proton Driver:** Provides 1–4 MW of protons on target from an upgraded AGS; a new booster at Fermilab would perform equivalently.

- **Target and Capture:** A high-power target immersed in a 20 T superconducting solenoidal field to capture pions produced in proton-nucleus interactions. The high magnetic field at the target is smoothly tapered down to a much lower value, 1.75 T, which is then maintained through the bunching and phase rotation sections of the Neutrino Factory.

- **Bunching and Phase Rotation:** We first accomplish the bunching with rf cavities of modest gradient, whose frequencies change as we proceed down the beam line. After bunching the beam, another set of rf cavities, with higher gradients and again having decreasing frequencies as we proceed down the beam line, is used to rotate the beam in longitudinal phase space to reduce its energy spread.

- **Cooling:** A solenoidal focusing channel, with high-gradient 201.25 MHz rf cavities and LiH absorbers, cools the transverse normalized rms emittance from 17 mm·rad to

about 7 mm·rad. This takes place at a central muon momentum of 220 MeV/c.

- **Acceleration:** A superconducting linac with solenoidal focusing is used to raise the muon beam energy to 1.5 GeV, followed by a Recirculating Linear Accelerator (RLA), arranged in a *dogbone* geometry, to provide a 5 GeV muon beam. Thereafter, a pair of cascaded Fixed-Field, Alternating Gradient (FFAG) rings, using a double lattice of combined-function magnets, is used to reach 20 GeV. Additional FFAG stages could be added to reach a higher beam energy, if the physics requires this.

- **Storage Ring:** We employ a compact racetrack-shaped superconducting storage ring in which $\approx 35\%$ of the stored muons decay toward a detector located some 3000 km from the ring. Muons survive for roughly 500 turns.

A. Proton Driver

The proton driver considered in FS2, and taken here as well, is an upgrade of the BNL Alternating Gradient Synchrotron (AGS) and uses most of the existing components and facilities; parameters are listed in Table I. To serve as the proton driver for a Neutrino Factory, the existing booster would be replaced by a 1.2 GeV superconducting proton linac. The modified layout is shown in Fig. 1. The AGS repetition rate would be increased from

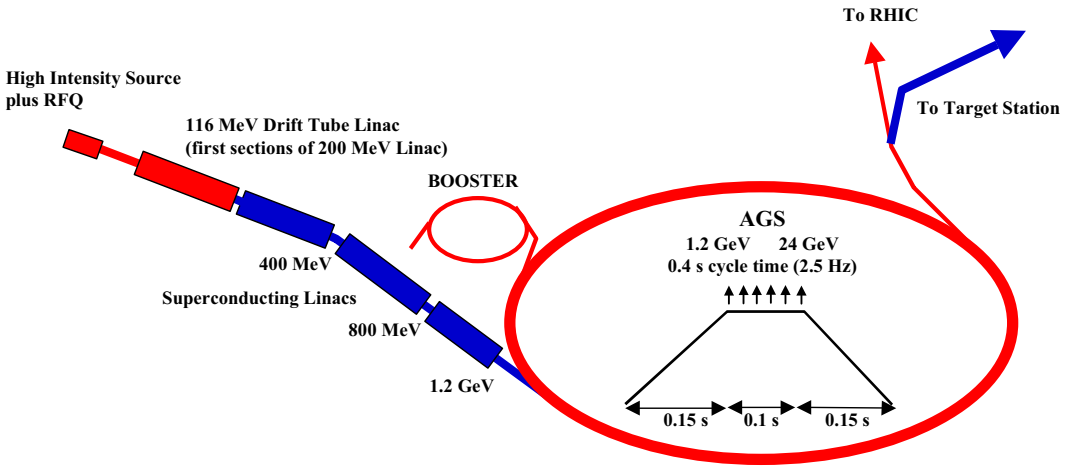

FIG. 1: (Color) AGS proton driver layout.

0.5 Hz to 2.5 Hz by adding power supplies to permit ramping the ring more quickly. No new technology is required for this—the existing supplies would be replicated and the magnet

strings would be split into six sectors rather than the two used presently. The total proton charge, 10^{14} ppp (protons per pulse) in six bunches, is only 40% higher than the current performance of the AGS. However, the bunches required for a Neutrino Factory are shorter than those used in the AGS at present, so there is a large increase in peak current and concomitant need for an improved vacuum chamber; this is included in the upgrade. The six bunches are extracted separately, spaced by 20 ms, so that the target and rf systems that follow need only deal with single bunches at an instantaneous repetition rate of 50 Hz (average rate of 15 Hz). The average proton beam power is 1 MW. A possible future upgrade to 2×10^{14} ppp and 5 Hz could give an average beam power of 4 MW. At this higher intensity, a superconducting bunch compressor ring would be needed to maintain the rms bunch length at 3 ns.

If the facility were built at Fermilab, the proton driver would be newly constructed. A number of technical options are presently being explored [11],[12].

TABLE I: Proton driver parameters for BNL design.

AGS	
Total beam power (MW)	1
Beam energy (GeV)	24
Average beam current (μA)	42
Cycle time (ms)	400
Number of protons per fill	1×10^{14}
Average circulating current (A)	6
No. of bunches per fill	6
No. of protons per bunch	1.7×10^{13}
Time between extracted bunches (ms)	20
Bunch length at extraction, rms (ns)	3

B. Target and Capture

A mercury-jet target is chosen to give a high yield of pions per MW of incident proton power. The 1-cm-diameter jet is continuous, and is tilted 100 mrad with respect to the

magnet axis, and the proton beam is tilted 66 mrad as well. The target layout is shown in Fig. 2. We assume that the thermal shock from the interacting proton bunch fully disperses

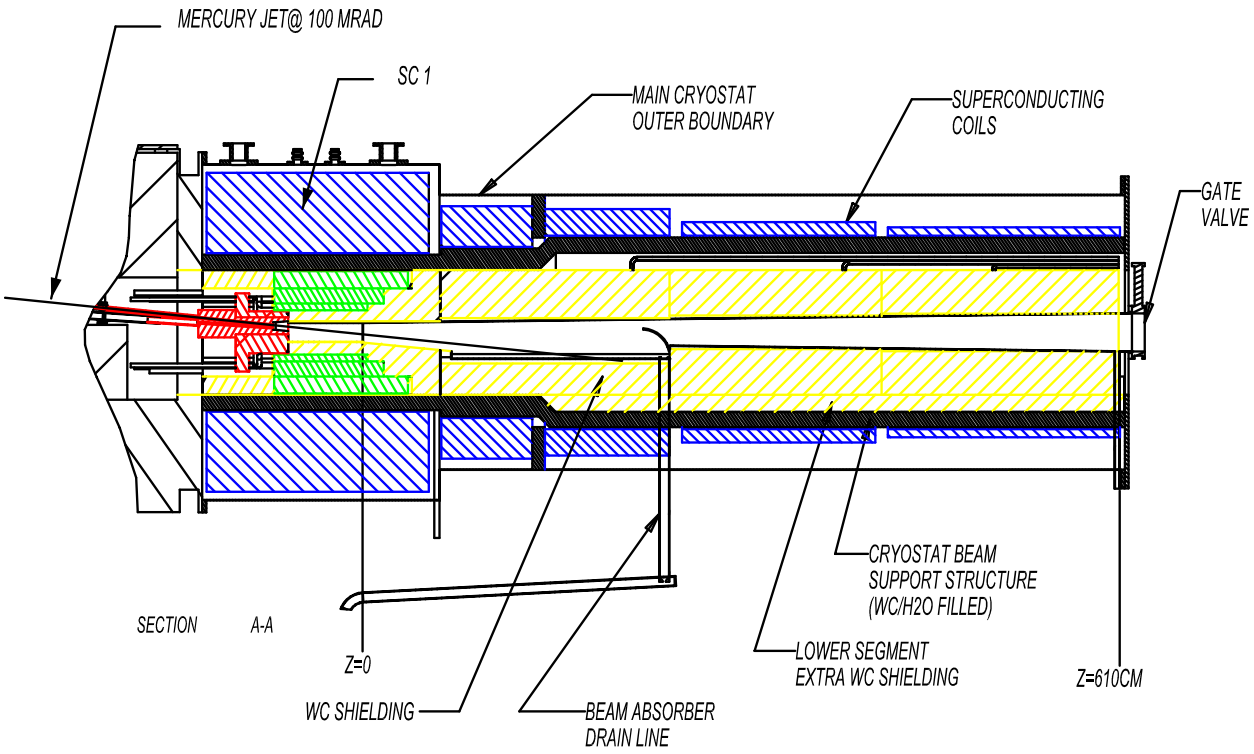

FIG. 2: (Color) Target, capture solenoids and mercury containment.

the mercury, so the jet must have a velocity of 20–30 m/s to allow the target material to be renewed before the next proton bunch arrives. Calculations of pion yields that reflect the detailed magnetic geometry of the target area have been performed with the MARS code [13] and are being used in the simulations reported in Section V. The FS2 design was updated for the present study to improve muon throughput. To avoid mechanical fatigue problems, a mercury pool serves as the beam dump. This pool is part of the overall target system—its mercury is circulated through the mercury jet nozzle after passing through a heat exchanger. Pions emerging from the target are captured and focused down the decay channel by a solenoidal field that is 20 T at the target center, and tapers down, over 12 m, to 1.75 T. The 20 T solenoid, with a resistive magnet insert and superconducting outer coil, is similar in character to higher field (up to 45 T), but smaller bore, magnets existing at several laboratories [14]. The magnet insert is made with hollow copper conductor having ceramic insulation to withstand radiation. MARS simulations [15] of radiation levels show that, with the shielding provided, both the copper and superconducting magnets will have

reasonable lifetime (see Section V).

C. Buncher and Phase Rotation

Pions, and the muons into which they decay, are generated in the target over a very wide range of energies, but in a short time pulse ($\approx$ 3 ns rms). To prepare the muon beam for acceleration thus requires significant *conditioning*. First, the bunch is drifted to develop an energy correlation, with higher energy particles at the head and lower energy particles at the tail of the bunch. Next, the long bunch is separated into a number of shorter bunches suitable for capture and acceleration in a 201-MHz rf system. This is done with a series of rf cavities having frequencies that decrease and gradients that increase along the beam line, separated by suitably chosen drift spaces. The resultant bunch train still has a substantial energy correlation, with the higher energy bunches first and progressively lower energy bunches coming behind. The large energy tilt is then *phase rotated*, using additional rf cavities of decreasing frequencies but constant gradient and drifts, into a bunch train with a longer time duration and a lower energy spread. The beam at the end of the buncher and phase rotation section has an average momentum of about 220 MeV/c. The proposed system is based on standard rf technology, and is expected to be much more cost effective than the induction-linac-based system considered in Ref. [9]. An additional benefit of the rf-based system is the ability to transport both signs of muon simultaneously.

D. Cooling

Transverse emittance cooling is achieved by lowering the beam energy in LiH absorbers, interspersed with rf acceleration to keep the average longitudinal momentum constant. Both transverse and longitudinal momenta are lowered in the absorbers, but only the longitudinal momentum is restored by the rf system. The emittance increase from Coulomb scattering in the absorbers is controlled by maintaining the focusing strength such that the angular spread of the beam at the absorber locations is reasonably large. In the present cooling lattice, the energy absorbers are attached directly to the apertures of the rf cavity, thus serving the dual purposes of closing the cavity apertures electromagnetically (increasing the cavity shunt impedance) and providing energy loss. Compared with the approach used

in FS2, the absorbers are more distributed, and do not lend themselves to being located at an optical focus. Therefore, the focusing is kept essentially constant along the cooling channel, but at a beta function somewhat higher than the minimum value achieved in FS2. A simple Focus-Focus (FOFO) lattice is employed. The solenoidal fields in each half-cell alternate in sign, giving rise to a sinusoidal field variation along the channel. Use of solid absorbers instead of the liquid-hydrogen absorbers assumed in FS2 will considerably simplify the cooling channel, and the new magnet requirements are also more modest, since fewer and weaker components are needed compared with FS2. Together, these features reduce the cost of the cooling channel with respect to the FS2 design. Although the cooling performance is reduced, the overall throughput is comparable to that in FS2 due to the increased acceptance built into the downstream acceleration system. Here too, the ability to utilize both signs of muons is available.

E. Acceleration

Parameters of the acceleration system are listed in Table II. A matching section, using a combination of normal conducting and superconducting rf cavities, matches the cooling channel optics to the requirements of a superconducting rf linac with solenoidal focusing which raises the energy to 1.5 GeV. This linac contains three parts (see Section V). The first part has only a single-cell 201 MHz cavity per period. The second part, with longer period, has a 2-cell rf cavity unit per period. The third part, as a still longer period becomes possible, accommodates two 2-cell cavity units per period. Figure 3 shows the three cryomodule types that make up the pre-accelerator linac.

The superconducting rf linac is followed by a 3.5-pass *dogbone* RLA, shown in Fig. 4, that raises the energy from 1.5 to 5 GeV. This RLA uses four 2-cell superconducting rf cavity structures per cell, and utilizes quadrupole triplet (as opposed to solenoidal) focusing.

Following the RLA are two cascaded FFAG rings that increase the beam energy from 5–10 GeV, and 10–20 GeV, respectively. Each ring uses combined-function magnets arranged in a doublet focusing arrangement. The lower energy FFAG ring has a circumference of about 286 m; the higher energy ring is about 400 m in circumference. As discussed in Section V, an effort was made to achieve a reasonably cost-optimized design. Without detailed engineering, it is not possible to fully optimize costs, but we have employed general formulae that properly

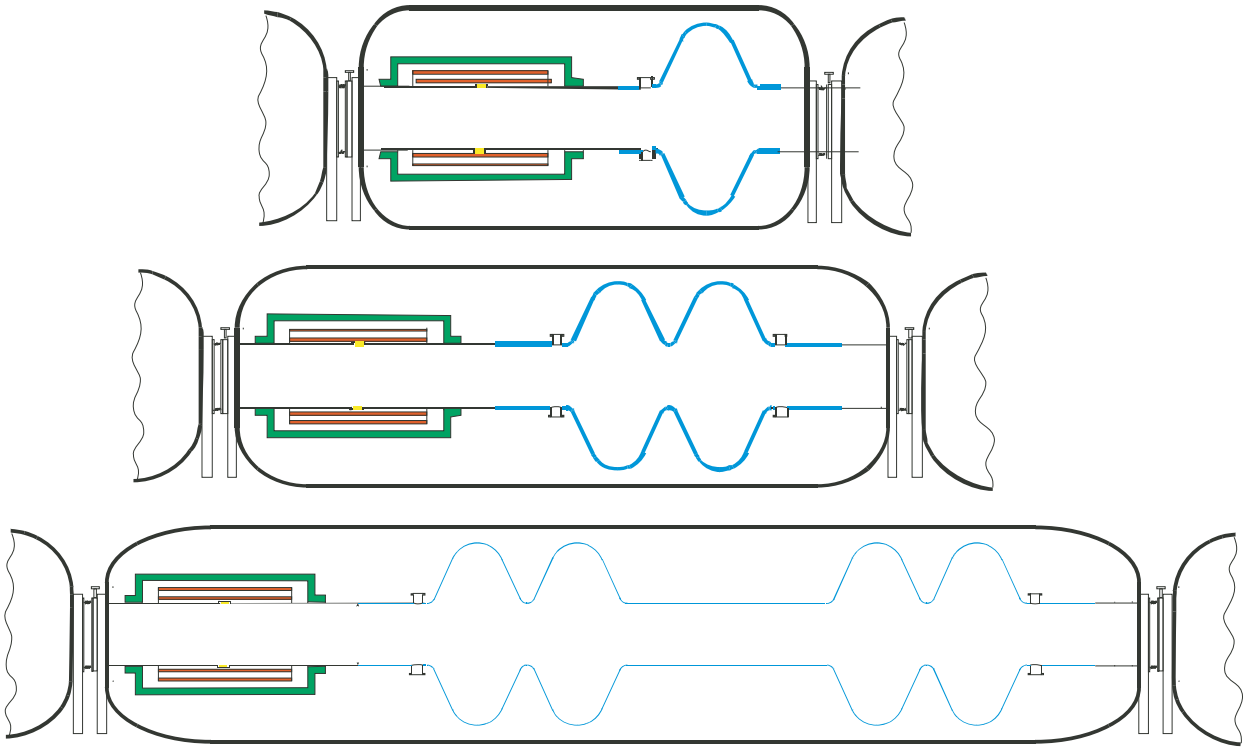

FIG. 3: (Color) Layouts of superconducting linac pre-accelerator cryomodules. Blue lines are the SC walls of the cavities and solenoid coils are indicated in red with the iron shielding in green.

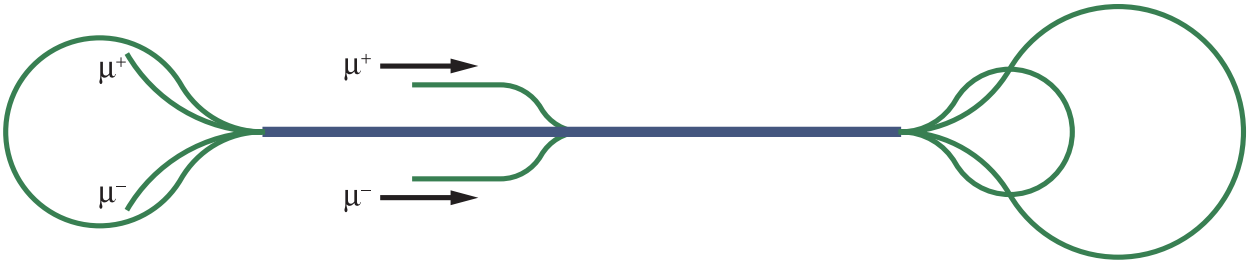

FIG. 4: (Color) Layout of the RLA.

represent the cost trends and that were considered adequate to make choices at the present stage of the design. As the acceleration system was one of the dominant cost items in FS2, we are confident that the approach adopted here will result in a less expensive Neutrino Factory facility with essentially the same performance as calculated for the FS2 design. Achieving a higher beam energy would require additional FFAG acceleration stages.

TABLE II: Important parameters for muon acceleration

Injection momentum (MeV/c)	273
Injection kinetic energy (MeV)	187
Final total energy (GeV)	20
Initial normalized acceptance (mm-rad)	30
rms normalized emittance (mm-rad)	3.84
Initial longitudinal acceptance, $\Delta p L_b/m_\mu c$ (mm)	150
Total energy spread, ΔE (MeV)	$\pm$45.8
Total time-of-flight (ns)	$\pm$1.16
rms energy spread (MeV)	19.8
rms time-of-flight (ns)	0.501
Number of bunches per pulse	89
Peak number of particles per bunch	1.1×10^{11}
Number of particles per pulse (per charge)	3×10^{12}
Bunch frequency/accelerating frequency (MHz)	201.25/201.25
Average beam power (per charge) (kW)	144

F. Storage Ring

After acceleration in the final FFAG ring, the muons are injected into the upward-going straight section of a racetrack-shaped storage ring with a circumference of 358 m. Parameters of the ring are summarized in Table III. High-field superconducting arc magnets are used to minimize the arc length and maximize the fraction (35%) of muons that decay in the downward-going straight, generating neutrinos headed toward the detector located some 3000 km away.

All muons are allowed to decay; the maximum heat load from their decay electrons is 42 kW (126 W/m). This load is too high to be dissipated in the superconducting coils. For FS2, a magnet design was chosen that allows the majority of these electrons to exit between separate upper and lower cryostats, and be dissipated in a dump at room temperature. To maintain the vertical cryostat separation in focusing elements, skew quadrupoles are employed in place of standard quadrupoles. In order to maximize the average bending field,

TABLE III: Muon storage ring parameters.

Energy (GeV)	20
Circumference (m)	358.18
Normalized transverse acceptance (mm-rad)	30
Energy acceptance (%)	2.2
Arc	
Length (m)	53.09
No. cells per arc	10
Cell length (m)	5.3
Phase advance (deg)	60
Dipole length (m)	1.89
Dipole field (T)	6.93
Skew quadrupole length (m)	0.76
Skew quadrupole gradient (T/m)	35
$\beta_{\max}$ (m)	8.6
Production Straight	
Length (m)	126
$\beta_{\max}$ (m)	200

Nb_3Sn pancake coils are employed. One coil of the bending magnet is extended and used as one half of the previous (or following) skew quadrupole to minimize unused space. For site-specific reasons, the ring is kept above the local water table and is placed on a roughly 30-m-high berm. This requirement places a premium on a compact storage ring. In the present study, no attempt was made to revisit the design of the FS2 storage ring. For further technical details on this component, see FS2, Ref. [9].

The footprint of a Neutrino Factory is reasonably small, and such a machine would fit easily on the site of an existing laboratory.

III. NEUTRINO BEAM PROPERTIES

The most important neutrino oscillation physics questions that we wish to address in the coming decades require the study of $\nu_e \leftrightarrow \nu_\mu$ transitions in long baseline experiments. Conventional neutrino beams are almost pure ν_μ beams, which therefore permit the study of $\nu_\mu \to \nu_e$ oscillations. The experiments must look for ν_e charged-current (CC) interactions in a distant detector. Backgrounds that fake ν_e CC interactions, together with a small ν_e component in the initial beam, account for $O(1\%)$ of the total interaction rate. This makes difficult, using conventional neutrino beams, to probe very small oscillation amplitudes, below the $0.01 - 0.001$ range. This limitation motivates new types of neutrino facilities, e.g. Neutrino Factory, that provide ν_e beams, permitting the search for $\nu_e \to \nu_\mu$ oscillations, and if the beam energy is above the ν_τ CC interaction threshold, the search for $\nu_e \to \nu_\tau$ oscillations.

A. Neutrino Factory Beams

Neutrino Factory beams are produced from muons decaying in a storage ring with long straight sections. Consider an ensemble of polarized negatively-charged muons. When the μ^- decay they produce ν_μ and $\bar{\nu}_e$ with distributions of energies and angles in the muon laboratory frame described by [16]:

$$\frac{d^2N_{\nu_\mu}}{dx d\Omega_{lab}} \propto \frac{1}{\gamma^2(1-\beta\cos\theta_{lab})^2}\frac{2x^2}{4\pi}\left[(3-2x)+(1-2x)P_\mu\cos\theta_{c.m.}\right], \tag{2a}$$

$$\frac{d^2N_{\bar{\nu}_e}}{dx d\Omega_{lab}} \propto \frac{1}{\gamma^2(1-\beta\cos\theta_{lab})^2}\frac{12x^2}{4\pi}\left[(1-x)+(1-x)P_\mu\cos\theta_{c.m.}\right] \tag{2b}$$

where $x \equiv 2E_\nu/m_\mu$, $\theta_{c.m.}$ is the angle between the neutrino momentum vector and the muon spin direction, and P_μ is the average muon polarization along the beam direction. The corresponding distributions for $\bar{\nu}_\mu$ and ν_e from μ^+ decay are obtained by the replacement $P_\mu \to -P_\mu$. Only neutrinos and antineutrinos emitted in the forward direction ($\cos\theta_{lab} \simeq 1$) are relevant to the neutrino flux for long-baseline experiments; in this limit $E_\nu = xE_{max}$ and at high energies the maximum E_ν in the laboratory frame is given by $E_{max} = \gamma(1 + \beta\cos\theta_{c.m.})m_\mu/2$, where β and γ are the usual relativistic factors. Thus, for a high energy muon beam with no beam divergence, the neutrino and antineutrino energy and angular distributions depend upon the parent muon energy, the decay angle, and the direction of

the muon spin vector. With the muon beam intensities that could be provided by a muon–collider type muon source [3] the resulting neutrino fluxes at a distant site would be large. For example, Fig. 5 shows as a function of muon energy and polarization, the computed fluxes per 2×10^{20} muon decays at a site on the other side of the Earth ($L = 10000$ km). Note that the ν_e ($\bar{\nu}_e$) fluxes are suppressed when the muons have $P = +1\,(-1)$. This can be understood by examining Eq. (2b) and noting that for $P = -1$ the two terms cancel in the forward direction for all x. At low energies, the neutrino CC interaction cross section is

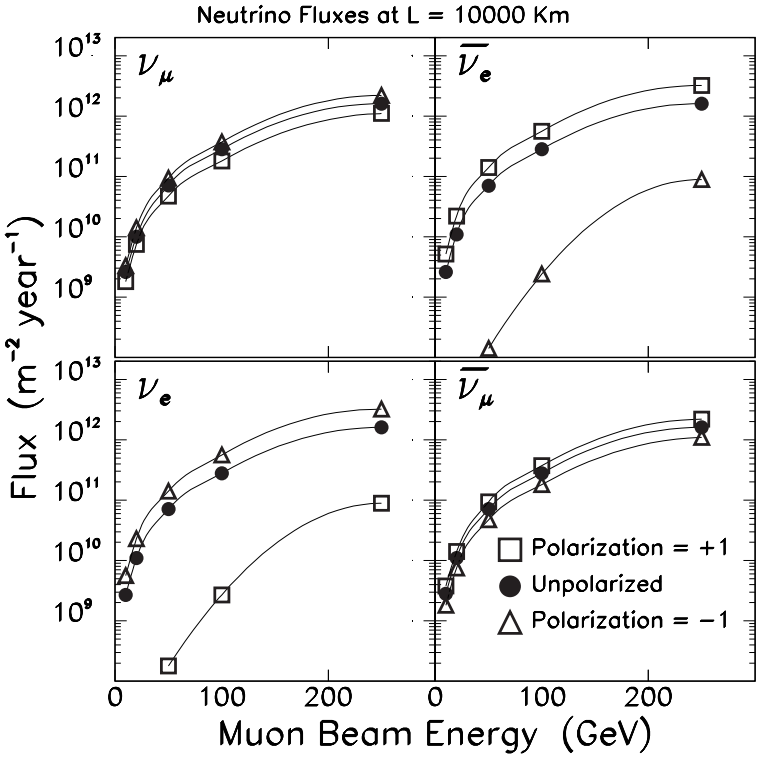

FIG. 5: Calculated ν and $\bar{\nu}$ fluxes in the absence of oscillations at a far site located 10000 km from a Neutrino Factory in which 2×10^{20} muons have decayed in the storage ring straight section pointing at the detector. The fluxes are shown as a function of the energy of the stored muons for negative muons (top two plots) and positive muons (bottom two plots), and for three muon polarizations as indicated. The calculated fluxes are averaged over a circular area of radius 1 km at the far site. Calculation from Ref. [2].

dominated by quasi-elastic scattering and resonance production. However, if E_ν is greater than $\sim$ 10 GeV, the total cross section is dominated by deep inelastic scattering and is

approximately [17]:

$$\sigma(\nu + N \to \ell^- + X) \approx 0.67 \times 10^{-38} \times E_\nu(\mathrm{GeV})\,\mathrm{cm}^2\,, \tag{3a}$$

$$\sigma(\overline{\nu} + N \to \ell^+ + X) \approx 0.34 \times 10^{-38} \times E_{\overline{\nu}}(\mathrm{GeV})\,\mathrm{cm}^2. \tag{3b}$$

The number of ν and $\bar{\nu}$ CC events per incident neutrino observed in an isoscalar target is given by:

$$N(\nu + N \to \ell^- + X) = 4.0 \times 10^{-15} \times E_\nu(\mathrm{GeV}) \text{ events per g/cm}^2, \tag{4a}$$

$$N(\overline{\nu} + N \to \ell^+ + X) = 2.0 \times 10^{-15} \times E_{\overline{\nu}}(\mathrm{GeV}) \text{ events per g/cm}^2. \tag{4b}$$

Using this simple form for the energy dependence of the cross section, the predicted energy

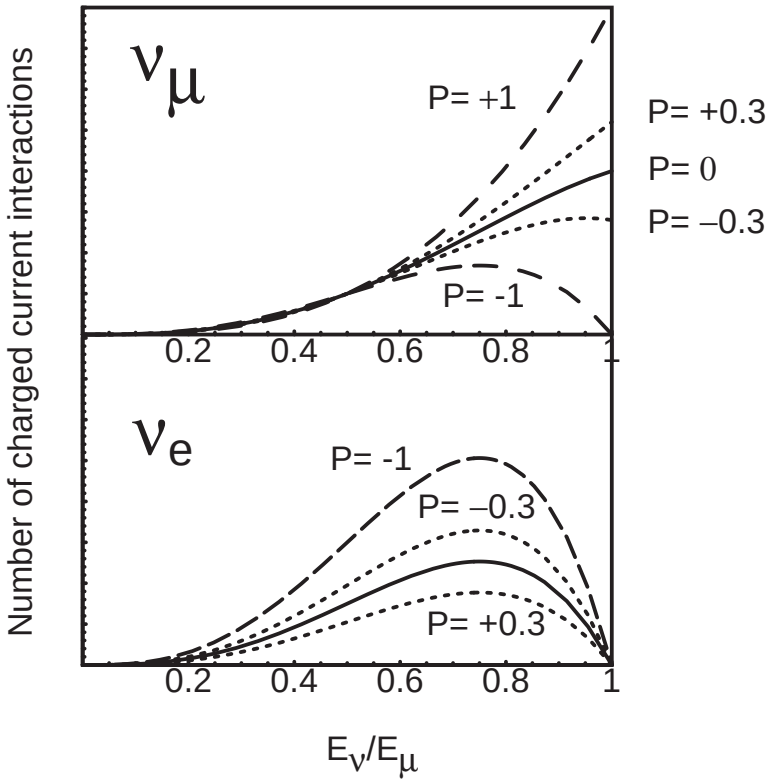

FIG. 6: Charged current event spectra at a far detector. The solid lines indicate zero polarization, the dotted lines indicate polarization of ± 0.3 and the dashed lines indicate full polarization. The $P = 1$ case for electron neutrinos results in no events and is hidden by the x axis.

distributions for ν_e and ν_μ interacting in a far detector ($\cos\theta = 1$) at a Neutrino Factory are shown in Fig. 6. The interacting ν_μ energy distribution is compared in Fig. 7 with the corresponding distribution arising from the high–energy NUMI [18] wide-band beam. Note

that neutrino beams from a Neutrino Factory have no high energy tail, and in that sense can be considered narrow-band beams.

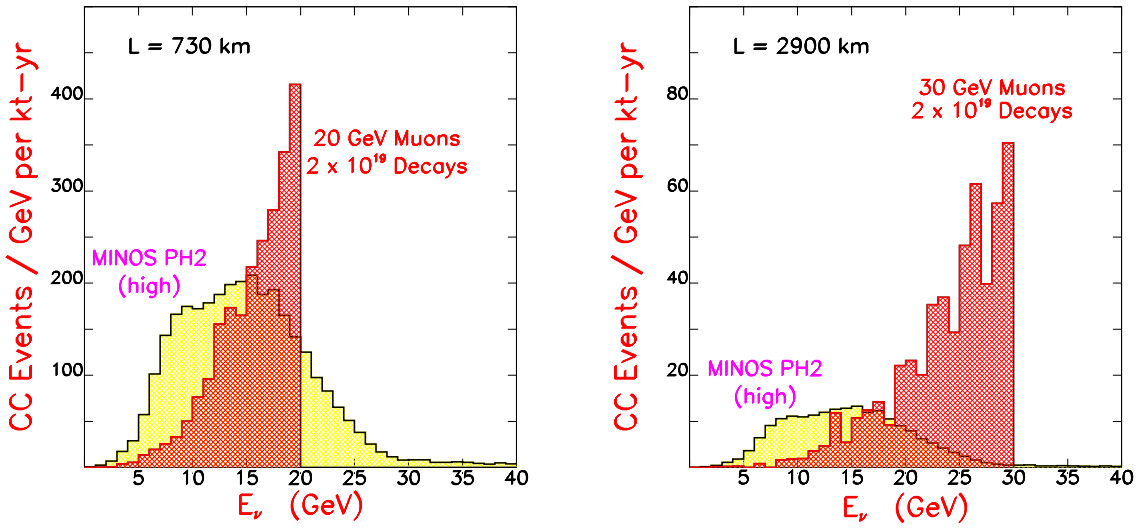

FIG. 7: (Color) Comparison of interacting ν_μ energy distributions for the NUMI high energy wide-band beam (Ref. [18]) with a 20 GeV Neutrino Factory beam (Ref. [2]) at $L = 730$ km and a 30 GeV Neutrino Factory beam at $L = 2900$ km. The Neutrino Factory distributions have been calculated based on Eq. (2) (no approximations), and include realistic muon beam divergences and energy spreads.

In practice, CC interactions can only be cleanly identified when the final state lepton exceeds a threshold energy. The calculated final state lepton distributions are shown in Fig. 8. Integrating over the energy distribution, the total ν and $\bar{\nu}$ interaction rates per muon decay are given by:

$$N_\nu \;=\; 1.2\times 10^{-14}\left[\frac{E_\mu^3(\mathrm{GeV})}{L^2(km)}\right]\times C(\nu)\;\;\text{events per kton,} \tag{5a}$$

$$N_{\bar{\nu}} \;=\; 0.6\times 10^{-14}\left[\frac{E_\mu^3(\mathrm{GeV})}{L^2(km)}\right]\times C(\nu)\;\;\text{events per kton}\,, \tag{5b}$$

where

$$C(\nu_\mu)=\frac{7}{10}+P_\mu\frac{3}{10}\quad,\quad C(\nu_e)=\frac{6}{10}-P_\mu\frac{6}{10}. \tag{6}$$

The calculated ν_e and ν_μ CC interaction rates resulting from 10^{20} muon decays in the storage ring straight section of a Neutrino Factory are compared in Table IV with expectations for the corresponding rates at the next generation of accelerator–based neutrino experiments.

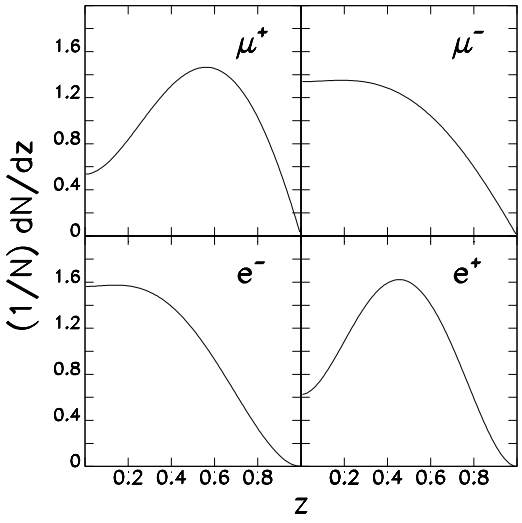

FIG. 8: Lepton energy spectra for CC $\bar{\nu}_\mu$ (top left), ν_μ (top right), ν_e (bottom left), and $\bar{\nu}_e$ (bottom right) interactions. Note that z is the energy normalized to the primary muon energy $z = E_\ell/E_\mu$. Calculation from Ref. [19].

Note that event rates at a Neutrino Factory increase as E_μ^3, and are significantly larger than expected for the next generation of approved experiments if $E_\mu > 20$ GeV. The radial dependence of the event rate is shown in Fig. 9 for a 20 GeV Neutrino Factory and three baselines.

1. Systematic Uncertainties

We next consider the systematic uncertainties on the neutrino flux. Since muon decay kinematics is very well understood, and the beam properties of the muons in the storage ring can be well determined, we expect the systematic uncertainties on the neutrino beam intensity and spectrum to be small compared to the corresponding uncertainties on the properties of conventional neutrino beams. In the muon decay straight section of a Neutrino Factory, the muon beam is designed to have an average divergence given by $\sigma_\theta = O(\frac{0.1}{\gamma})$. The neutrino beam divergence will therefore be dominated by muon decay kinematics, and uncertainties on the beam direction and divergence will yield only small uncertainties in the neutrino flux at a far site. However, if precise knowledge of the flux is required, the uncertainties on θ and σ_θ must be taken into account, along with uncertainties on the flux

TABLE IV: Muon neutrino and electron antineutrino CC interaction rates in the absence of oscillations, calculated for baseline length $L = 732$ km (FNAL $\rightarrow$ Soudan), for MINOS using the wide-band beam and a muon storage ring delivering 10^{20} decays with $E_\mu = 10, 20$, and 50 GeV at three baselines. The Neutrino Factory calculation includes a realistic muon beam divergence and energy spread.

Experiment		Baseline (km)	$\langle E_{\nu_\mu} \rangle$ (GeV)	$\langle E_{\bar{\nu}_e} \rangle$ (GeV)	N(ν_μ CC) (per kton-yr)	N($\bar{\nu}_e$ CC) (per kton-yr)
MINOS	Low energy	732	3	–	458	1.3
	Medium energy	732	6	–	1439	0.9
	High energy	732	12	–	3207	0.9
Muon ring	E_μ (GeV)					
	10	732	7.5	6.6	1400	620
	20	732	15	13	12000	5000
	50	732	38	33	1.8×10^5	7.7×10^4
Muon ring	E_μ (GeV)					
	10	2900	7.6	6.5	91	41
	20	2900	15	13	740	330
	50	2900	38	33	11000	4900
Muon ring	E_μ (GeV)					
	10	7300	7.5	6.4	14	6
	20	7300	15	13	110	51
	50	7300	38	33	1900	770

arising from uncertainties on the muon energy distribution and polarization. The relationships between the uncertainties on the muon beam properties and the resulting uncertainties on the neutrino flux are summarized in Table V. If, for example, we wish to know the ν_e and ν_μ fluxes at a far site with a precision of 1%, we must determine the beam divergence, σ_θ, to 20% (see, Fig. 10), and ensure that the beam direction is within $0.6 \times \sigma_\theta$ of the nominal direction [20] (see, Fig. 11). We point out that it should be possible to do much better than this, and consequently, to know the fluxes at the far site with a precision much better than

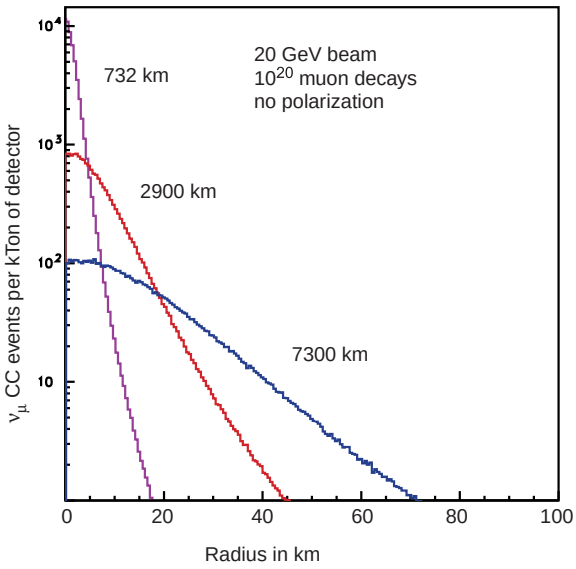

FIG. 9: (Color) Events per kton of detector as a function of distance from the beam center for a 20 GeV muon beam.

TABLE V: Dependence of predicted charged current event rates on muon beam properties at a Neutrino Factory. The last column lists the required precisions with which each beam property must be determined if the uncertainty on the neutrino flux at the far site is to be less than $\sim 1\%$. Here Δ denotes uncertainty while σ denotes the spread in a variable. Table from Ref. [20].

Muon Beam property	Beam Type	Rate Dependence	Target Precision
Energy (E_μ)	ν (no osc.)	$\Delta N/N = 3\ \Delta E_\mu/E_\mu$	$\Delta(E_\mu)/E_\mu < 0.003$
	$\nu_e \to \nu_\mu$	$\Delta N/N = 2\ \Delta E_\mu/E_\mu$	$\Delta(E_\mu)/E_\mu < 0.005$
Direction ($\Delta\theta$)	ν (no osc.)	$\Delta N/N \leq 0.01$ (for $\Delta\theta < 0.6\ \sigma_\theta$)	$\Delta\theta < 0.6\ \sigma_\theta$
Divergence (σ_θ)	ν (no osc.)	$\Delta N/N \sim 0.03\ \Delta\sigma_\theta/\sigma_\theta$ (for $\sigma_\theta \sim 0.1/\gamma$)	$\Delta\sigma_\theta/\sigma_\theta < 0.2$ (for $\sigma_\theta \sim 0.1/\gamma$)
Momentum spread (σ_p)	ν (no osc.)	$\Delta N/N \sim 0.06\ \Delta\sigma_p/\sigma_p$	$\Delta\sigma_p/\sigma_p < 0.17$
Polarization (P_μ)	ν_e (no osc.)	$\Delta N_{\nu_e}/N_{\nu_e} = \Delta P_\mu$	$\Delta P_\mu < 0.01$
	ν_μ (no osc.)	$\Delta N_{\nu_\mu}/N_{\nu_\mu} = 0.4\ \Delta P_\mu$	$\Delta P_\mu < 0.025$

1%.

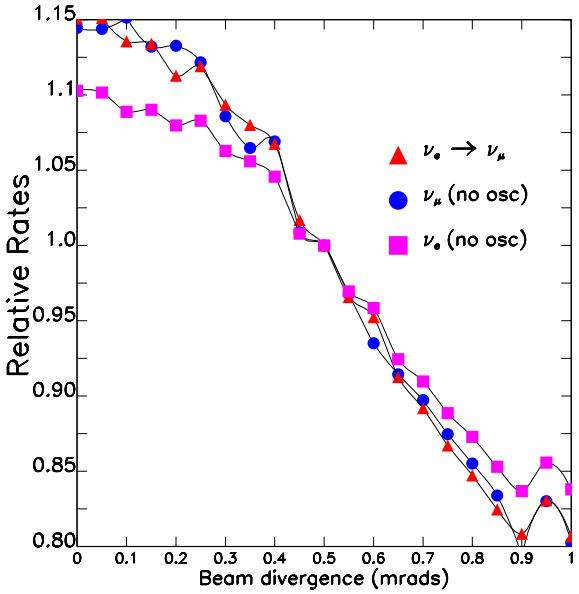

FIG. 10: (Color) Dependence of CC interaction rates on the muon beam divergence for a detector located at $L = 2800$ km from a muon storage ring containing 30 GeV unpolarized muons. Rates are shown for ν_e (boxes) and ν_μ (circles) beams in the absence of oscillations, and for $\nu_e \rightarrow \nu_\mu$ oscillations (triangles) with the three–flavor oscillation parameters, $\delta m^2_{12} = 5\times10^{-5}\,\mathrm{eV}^2/\mathrm{c}^4$, $\delta m^2_{32} = 3.5 \times 10^{-3}\,\mathrm{eV}^2/\mathrm{c}^4$, $s_{13} = 0.10$, $s_{23} = 0.71$, $s_{12} = 0.53$, $\delta = 0$. The calculation is from Ref. [20].

IV. NEUTRINO OSCILLATION PHYSICS REACH

Ultimately, to fully test the three-flavor mixing framework, determine all of the relevant neutrino oscillation parameters, and answer the most important neutrino-oscillation related physics questions, we would like to measure the oscillation probabilities $P(\nu_\alpha \rightarrow \nu_\beta)$ as a function of the baseline L and neutrino energy E (and hence L/E) for all possible initial and final flavors α and β. This requires a beam with a well known initial flavor content, and a detector that can identify the flavor of the interacting neutrino. The neutrinos interact in the detector via charged current (CC) and neutral current (NC) interactions to produce a lepton accompanied by a hadronic shower arising from the remnants of the struck nucleon. In CC interactions, the final-state lepton tags the flavor (β) of the interacting neutrino. To accomplish our ultimate goal, we will need ν_e in addition to ν_μ beams, and detectors that

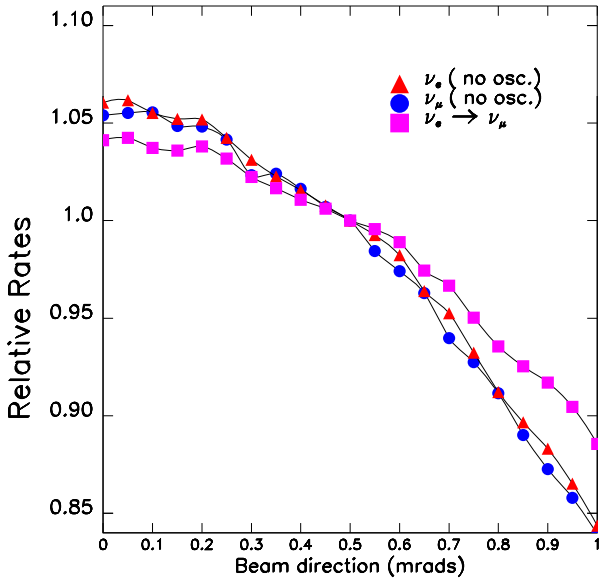

FIG. 11: (Color) Dependence of CC interaction rates on the neutrino beam direction. Relative rates are shown for a detector at a far site located downstream of a storage ring containing 30 GeV unpolarized muons, and a muon beam divergence of 0.33 mrad. Rates are shown for ν_e (triangles) and ν_μ (circles) beams in the absence of oscillations, and for $\nu_e \rightarrow \nu_\mu$ oscillations (boxes) with the three–flavor oscillation parameters shown in Fig. 10. The calculation is from Ref. [20].

can distinguish between NC, ν_e CC, ν_μ CC, and ν_τ CC interactions. Conventional neutrino beams are ν_μ beams, Beta Beams provide ν_e beams, and Neutrino Factories provide ν_e and ν_μ beams. The sensitivities of experiments at the different facilities will depend on their statistical precision, the background rates, the ability of the experiments to discriminate between true and false solutions within the three-flavor mixing parameter space, and the ability of the experimental setups to detect as many of the oscillation modes as possible. In the following, we will consider the experimental signatures and sensitivities at a Neutrino Factory.

A. Neutrino Factory Sensitivity

1. *Wrong-Sign Muons*

At a Neutrino Factory in which, for example, positive muons are stored, the initial beam consists of 50% ν_e and 50% $\bar{\nu}_\mu$. In the absence of oscillations, the ν_e CC interactions produce electrons and the $\bar{\nu}_\mu$ CC interactions produce positive muons. Note that the charge of the final state lepton tags the flavor of the initial neutrino or antineutrino. In the presence of $\nu_e \to \nu_\mu$ oscillations, the ν_μ CC interactions produce negative muons (i.e., wrong–sign muons). This is a very clean experimental signature since, with a segmented magnetized iron-scintillator sampling calorimeter for example, it is straightforward to suppress backgrounds to 1 part in 10^4 of the total CC interaction rate, or better. This means that at a Neutrino Factory backgrounds to the $\nu_e \to \nu_\mu$ oscillation signal are extremely small. The full statistical sensitivity can therefore be exploited down to values of $\sin^2 2\theta_{13}$ approaching 10^{-4} before backgrounds must be subtracted and further advances in sensitivity scale like $\sqrt{N}$ rather than N. This enables Neutrino Factories [21, 22] to go beyond the sensitivities achievable by conventional neutrino Superbeams, by about two orders of magnitude. A more complete discussion of backgrounds at a Neutrino Factory can be found in Refs. [23, 24].

We now consider how wrong-sign muon measurements at a Neutrino Factory are used to answer the most important neutrino oscillation physics questions. Suppose we store positive muons in the Neutrino Factory, and measure the number of events tagged by a negative muon in a distant detector, and then store negative muons and measure the rate of events tagged by a positive muon. To illustrate the dependence of the expected measured rates on the chosen baseline, the neutrino mass hierarchy, and the complex phase δ, we will fix the other oscillation parameters and consider an experiment downstream of a 20 GeV Neutrino Factory. Let half of the data taking be with μ^+ stored, and the other half with μ^- stored. In Fig. 12, the predicted ratio of wrong-sign muon events $R \equiv N(\bar{\nu}_e \to \bar{\nu}_\mu)/N(\nu_e \to \nu_\mu)$ is shown as a function of baseline for $\Delta m^2_{32} = +0.0035$ eV^2 and -0.0035 eV^2, with $\sin^2 2\theta_{13}$ set to the small value 0.004. (Although these Δm^2 values are now a little different from those emerging from global analyses of the atmospheric and solar neutrino data, they are the ones used for the figure, which comes from Ref. [25], and are still useful to illustrate how the measurements can be used to determine the oscillation parameters.) Figure 12 shows two bands. The upper

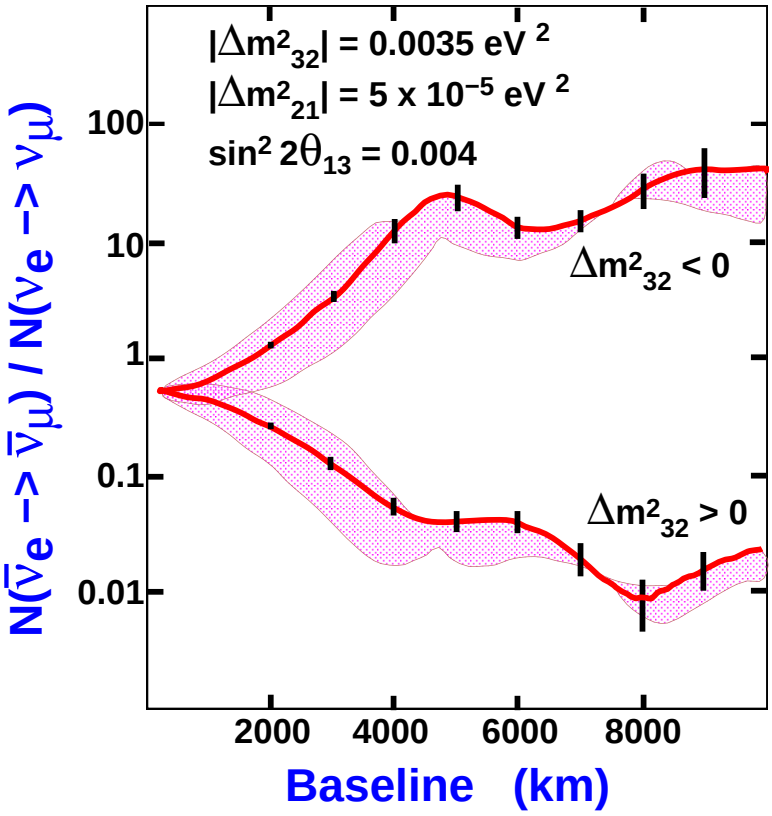

FIG. 12: (Color) Predicted ratios of wrong–sign muon event rates when positive and negative muons are stored in a 20 GeV Neutrino Factory, shown as a function of baseline. A muon measurement threshold of 4 GeV is assumed. The lower and upper bands correspond, respectively, to the two possible neutrino mass eigenstate orderings, as labeled. The widths of the bands show how the predictions vary as the *CP* violating phase δ is varied from $-\frac{\pi}{2}$ to $+\frac{\pi}{2}$, with the thick lines showing the predictions for $\delta = 0$. The statistical error bars correspond to a Neutrino Factory yielding a data sample of 10^{21} decays with a 50 kton detector. Figure from Ref. [25].

(lower) band corresponds to $\Delta m^2_{32} < 0\,(> 0)$. Within the bands, the *CP* phase δ is varying. At short baselines the bands converge, and the ratio $R = 0.5$ since the antineutrino CC cross section is half of the neutrino CC cross section. At large distances, matter effects enhance R if $\Delta m^2_{32} < 0$ and reduce R if $\Delta m^2_{32} > 0$, and the bands diverge. Matter effects become significant for baselines exceeding about 2000 km. The error bars indicate the expected statistical uncertainty on the measured R with a data sample of 5×10^{22} kton-decays. With these statistics, the sign of Δm^2_{32} is determined with very high statistical significance. With an order of magnitude smaller data sample (entry level scenario [26]) or with an order of

magnitude smaller $\sin^2 2\theta_{13}$ the statistical uncertainties would be $\sqrt{10}$ larger, but the sign of Δm^2_{32} could still be determined with convincing precision. In addition to the ratio of

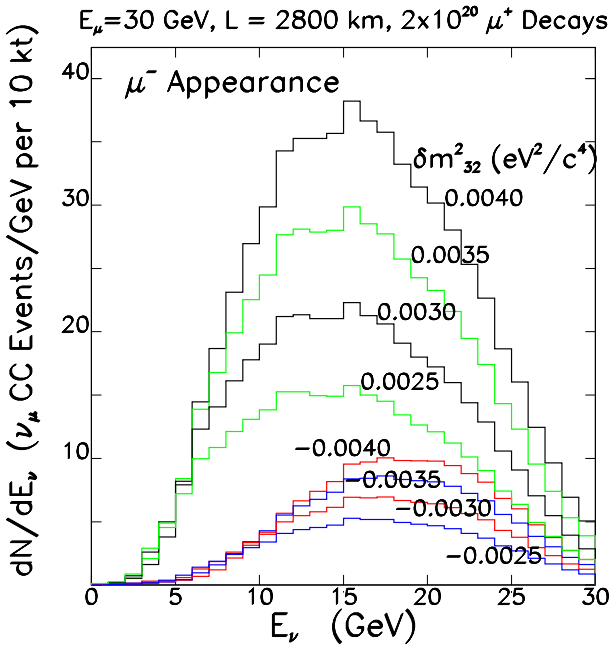

FIG. 13: (Color) Predicted measured energy distributions for CC events tagged by a wrong-sign (negative) muon from $\nu_e \to \nu_\mu$ oscillations (no cuts or backgrounds), shown for various δm^2_{32}, as labeled. The predictions correspond to 2×10^{20} decays, $E_\mu = 30$ GeV, $L = 2800$ km, and a representative set of values for δm^2_{12}, $\sin^2 2\theta_{13}$, $\sin^2 2\theta_{23}$, $\sin^2 2\theta_{12}$, and δ. Results are from Ref. [27].

wrong–sign muon signal rates R, the two energy-dependent wrong-sign muon event energy distributions can be separately measured. To show how this additional information can help, the predicted measured energy distributions 2800 km downstream of a 30 GeV Neutrino Factory are shown in Figs. 13 and 14 for, respectively, $\nu_e \to \nu_\mu$ and $\bar{\nu}_e \to \bar{\nu}_\mu$ wrong–sign muon events. The distributions are shown for a range of positive and negative values of δm^2_{32}. Note that, after allowing for the factor of two difference between the neutrino and antineutrino cross sections, for a given $|\delta m^2_{32}|$, if $\delta m^2_{32} > 0$ we would expect to observe a lower wrong–sign muon event rate and a harder associated spectrum when positive muons are stored in the Neutrino Factory than when negative muons are stored. On the other hand, if $\delta m^2_{32} < 0$ we would expect to observe a higher wrong–sign muon event rate and a softer associated spectrum when positive muons are stored in the Neutrino Factory than when negative muons are stored. Hence, measuring the differential spectra when positive

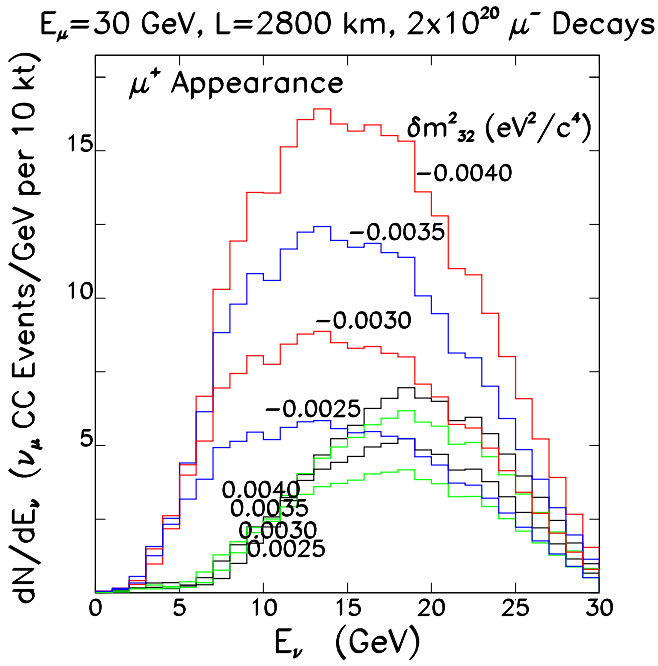

FIG. 14: (Color) Same as in Fig. 13, for CC events tagged by a wrong-sign (positive) muon from $\bar{\nu}_e \to \bar{\nu}_\mu$ oscillations.

and negative muons are alternately stored in the Neutrino Factory can both enable the sign of δm^2_{32} to be unambiguously determined [27], and also provide a measurement of δm^2_{32} and a consistency check between the behavior of the rates and energy distributions.

2. Other Channels

In practice, to measure θ_{13}, determine the mass hierarchy, and search for *CP* violation, the analysis of the wrong-sign muon rates must be performed allowing all of the oscillation parameters to simultaneously vary within their uncertainties. Since the relationship between the measured quantities and the underlying mixing parameters is complicated, with a minimal set of measurements it may not be possible to identify a unique region of parameter space consistent with the data. For Superbeams a detailed discussion of this problem can be found in Refs. [28, 29, 30, 31, 32, 33]. To understand the nature of the challenge, Fig. 15 shows, as a function of $\theta_{13}, \theta_{23}, \delta$ and the assumed mass hierarchy, the predicted number of wrong–sign muon events when negative muons are stored in the Neutrino Factory, versus the corresponding rate when positive muons are stored. The example is for a 16 GeV Neutrino

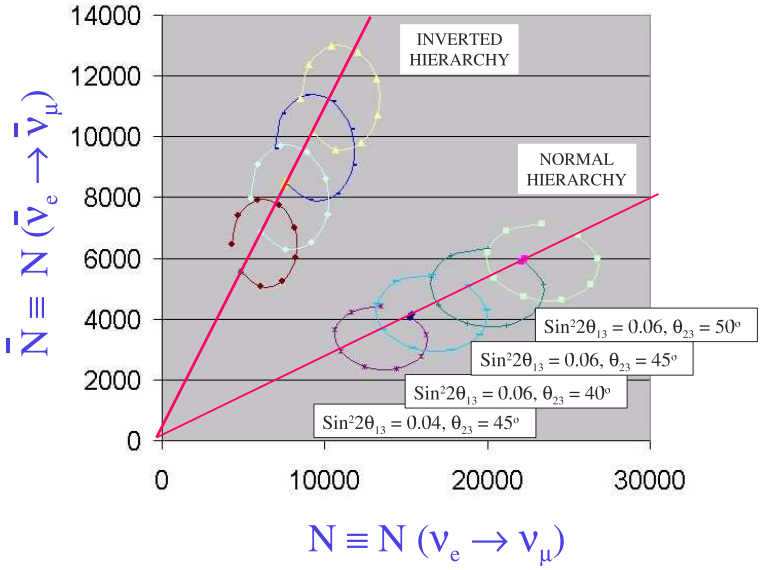

FIG. 15: (Color) The predicted number of wrong–sign muon events when negative muons are stored in the Neutrino Factory, versus the corresponding rate when positive muons are stored, shown as a function of $\theta_{13}, \theta_{23}, \delta$ and the assumed mass hierarchy, as labeled. The calculation corresponds to a 16 GeV Neutrino Factory with a baseline of 2000 km, and 10 years of data taking with a 100 kton detector and 2×10^{20} μ^+ and 2×10^{20} μ^- decays in the beam-forming straight section per year. The ellipses show how the predicted rates vary as the *CP* phase δ varies.

Factory with a baseline of 2000 km, and 10 years of data taking with a 100 kton detector and 2×10^{20} μ^+ and 2×10^{20} μ^- decays in the beam-forming straight section per year. The ellipses show how the predicted rates vary as the *CP* phase δ varies. All of the *CP* conserving points ($\delta = 0$ and π) lie on the diagonal lines. Varying the mixing angles moves the ellipses up and down the lines. Varying the mass hierarchy moves the family of ellipses from one diagonal line to the other. Note that the statistics are large, and the statistical errors would be barely visible if plotted on this figure. Given these statistical errors, for the parameter region illustrated by the figure, determining the mass hierarchy (which diagonal line is the measured point closest to) will be straightforward. Determining whether there is *CP* violation in the lepton sector will amount to determining whether the measured point is consistent with being on the *CP* conserving line. Determining the exact values for the mixing angles and δ is more complicated, since various combinations can result in the same

predicted values for the two measured rates. This is the origin of possible false solutions in the three–flavor mixing parameter space. To eliminate those false solutions, event samples other than $\nu_e \rightarrow \nu_\mu$ transitions tagged by wrong-sign muons will be important. We have seen that, in the presence of $\nu_e \rightarrow \nu_\mu$ oscillations, the ν_μ CC interactions produce negative muons (i.e., wrong–sign muons). Similarly, $\bar{\nu}_\mu \rightarrow \bar{\nu}_e$ oscillations produce wrong–sign electrons, $\bar{\nu}_\mu \rightarrow \bar{\nu}_\tau$ oscillations produce events tagged by a τ^+, and $\nu_e \rightarrow \nu_\tau$ oscillations produce events tagged by a τ^-. Hence, there is a variety of information that can be used to measure or constrain neutrino oscillations at a Neutrino Factory, namely the rates and energy distributions of events tagged by

(a) right–sign muons

(b) wrong–sign muons

(c) electrons or positrons (their charge is difficult to determine in a massive detector)

(d) positive τ–leptons

(e) negative τ–leptons

(f) no charged lepton.

If these measurements are made when there are alternately positive and negative muons decaying in the storage ring, there are a total of 12 spectra that can be used to extract information about the oscillations. Some examples of the predicted measured spectra are shown as a function of the oscillation parameters in Figs. 16 and 17 for a 10 kton detector sited 7400 km downstream of a 30 GeV Neutrino Factory. These distributions are sensitive to the oscillation parameters, and can be fit simultaneously to extract the maximum information. Clearly, the high intensity ν_e, $\bar{\nu}_e$, ν_μ, and $\bar{\nu}_\mu$ beams at a Neutrino Factory would provide a wealth of precision oscillation data. The full value of this wealth of information has not been fully explored, but some specific things to be noted are:

1. It has been shown [34, 35, 36, 37] that the various measurements at a Neutrino Factory provide sufficient information to eliminate false solutions within the three–flavor parameter space. Indeed the wealth of information in the Neutrino Factory data is essential for this purpose.

2. If $\sin^2 2\theta_{13}$ exceeds ~ 0.001 the $\nu_e \rightarrow \nu_\tau$ channel is particularly important, both as a means to suppress the false solutions [34, 38], and also as the only direct experimental probe of $\nu_e \leftrightarrow \nu_\tau$ transitions. The ability of the $\nu_e \rightarrow \nu_\tau$ measurements to eliminate false solutions is illustrated in Fig. 18, which, for a representative set of oscillation parameters, shows as a function of the *CP* phase δ the location of the false solution with respect to the correct solution in θ_{13}–space (or more precisely, the distance between the two solutions $\Delta\theta$). Note that, when compared to the $\bar{\nu_e} \rightarrow \bar{\nu_\mu}$ case, $\Delta\theta$ has the opposite sign for $\bar{\nu_e} \rightarrow \bar{\nu_\tau}$. In practice, this means that together the two measurements enable the false solution to be effectively eliminated.

3. Within the three–flavor framework, the relationship between the measured oscillation probabilities and the associated oscillation parameters is complicated. Experimental redundancy, permitting the over-determination of the oscillation parameters, is likely to prove essential, both to weed out misleading measurements and to ensure that the three-flavor framework is correct.

3. Neutrino Factory Calculations

To understand how sensitive Neutrino Factory measurements will be in determining θ_{13} and the neutrino mass hierarchy, and the sensitivity to *CP* violation in the lepton sector, we must consider the impact of statistical and systematic uncertainties, correlations between the parameters that vary within fits to the measured distributions, and the presence or absence of false solutions in the three-flavor mixing parameter space. To take account of these effects, and to see which different neutrino oscillation experiments best complement one another, a global fitting program has been created [36, 40] that uses simulated right-sign muon and wrong-sign muon data sets, and includes:

1. Beam spectral and normalization uncertainties.

2. Matter density variations of 5% about the average value.

3. Constraint of solar neutrino oscillation parameters within the post-KamLAND LMA region.

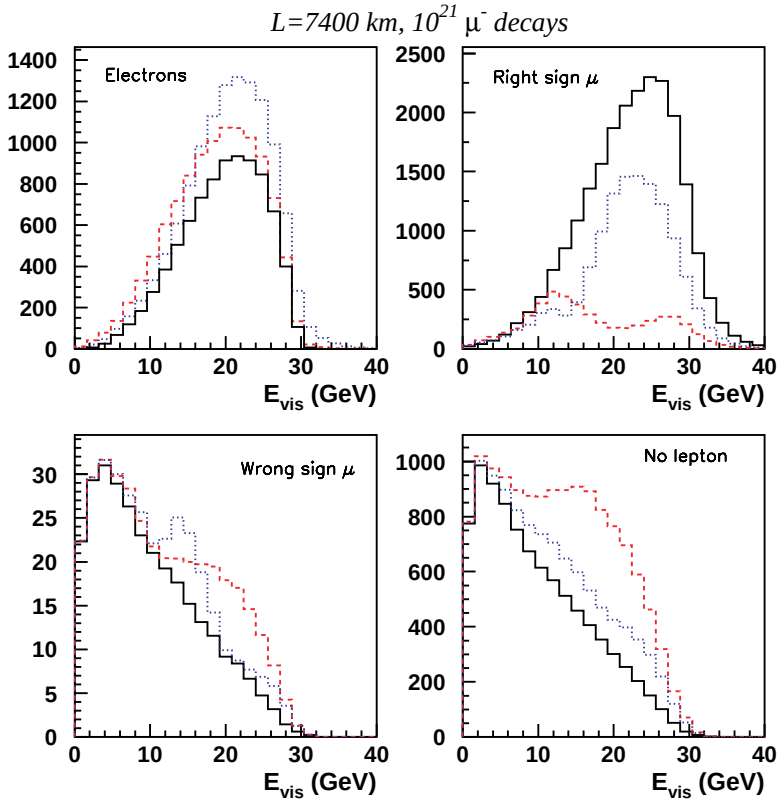

FIG. 16: (Color) Visible energy spectra for four event classes when $10^{21}\,\mu^-$ decay in a 30 GeV Neutrino Factory at $L = 7400$ km. Black solid histogram: no oscillations. Blue dotted histogram: $\delta m^2_{32} = 3.5 \times 10^{-3}$ eV^2/c^4, $\sin^2\theta_{23} = 1$. Red dashed histogram: $\delta m^2_{32} = 7 \times 10^{-3}$ eV^2/c^4, $\sin^2\theta_{23} = 1$. The distributions in this figure and the following figure are for an ICANOE-type detector, and are from Ref. [39].

4. Simulation of ν_μ CC QE, ν_μ and ν_e CC inelastic, and NC events for all flavors. Note that the NC events are included in the analysis as a source of background. The NC signal is not yet exploited as an additional constraint.

5. A check of the influence of cross section uncertainties (this mostly affects energies lower than those of interest for Neutrino Factories).

6. Energy-dependent detection efficiencies, enabling energy threshold effects to be taken into account.

7. Gaussian energy resolutions.

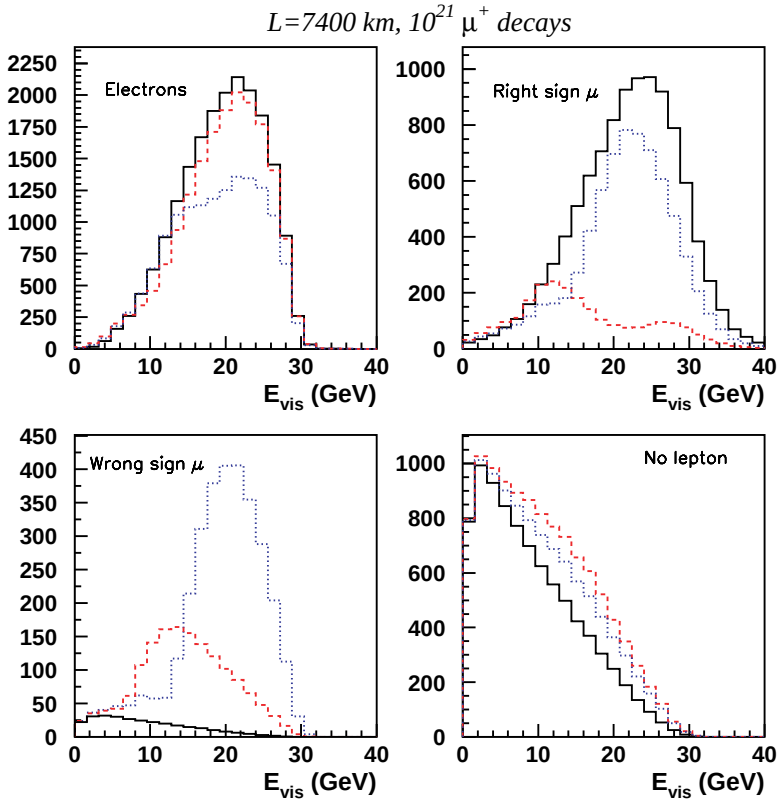

FIG. 17: (Color) Same as in Fig. 16, but with positive muons circulating in the storage ring. The difference between the two figures is due to the different cross section for neutrinos and antineutrinos, and to matter effects.

8. Flavor, charge, and event misidentification.

9. Overall energy-scale and normalization errors.

10. An analysis of statistical and systematic precisions, and the ability to eliminate false solutions.

The calculated signal and background rates are listed in Table VI. The roughly two orders of magnitude improvement in the signal/background ratio at a Neutrino Factory, compared with the corresponding ratio at a high performance Superbeam, is evident. The results from the full calculations are shown in Fig. 19. The calculation is more fully described in Ref. [36]. The figure shows the minimum value of $\sin^2 2\theta_{13}$ for which three experimental goals could be achieved (with 3σ significance). First, the observation of a finite value of θ_{13}. Second,

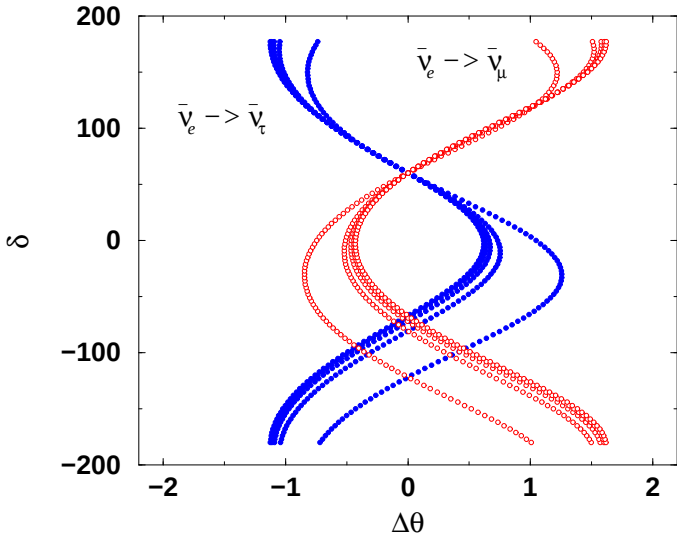

FIG. 18: (Color) Equiprobability curves in the $(\Delta\theta, \delta)$ plane, for $\bar{\theta}_{13} = 5°$, $\bar{\delta} = 60°$, $E_\nu \in [5, 50]$ GeV and $L = 732$ km for the $\nu_e \to \nu_\mu$ and $\nu_e \to \nu_\tau$ oscillation (neutrinos on the left, antineutrinos on the right). $\Delta\theta$ is defined as the difference between the reconstructed parameter θ_{13} and the input parameter $\bar{\theta}_{13}$, i.e., $\Delta\theta = \theta_{13} - \bar{\theta}_{13}$. From Ref. [34].

TABLE VI: Signal and background rates for a CERN SPS Beta Beam facility, a high performance Superbeam (a 4 MW JHF beam with a 1 Mton water Cerenkov detector), and a Neutrino Factory. The numbers correspond to $\sin^2 2\theta_{13} = 0.1$ and $\delta = 0$. The rates have been calculated by the authors of Ref. [36].

	β-Beam	JHF-HK	Nu-Factory
	ν		
Signal	4967	13171	69985
Background	397	2140	95.2
Signal/Background	12.5	6.2	735
	$\bar{\nu}$		
Signal	477	9377	15342
Background	1	3326	180
Signal/Background	477.5	2.8	85.2

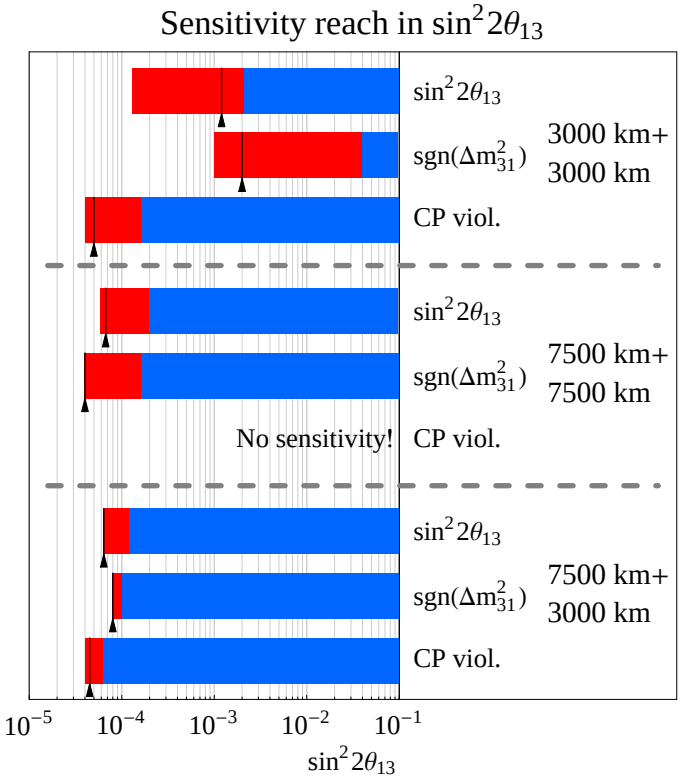

FIG. 19: (Color) The sensitivity reaches as functions of $\sin^2 2\theta_{13}$ for $\sin^2 2\theta_{13}$ itself, the sign of $\Delta m^2_{31} > 0$, and (maximal) *CP* violation $\delta_{\rm CP} = \pi/2$ for each of the indicated baseline combinations. The bars show the ranges in $\sin^2 2\theta_{13}$ where sensitivity to the corresponding quantity can be achieved at the 3σ confidence level. The dark bars mark the variations in the sensitivity limits by allowing the true value of Δm^2_{21} to vary in the 3σ LMA-allowed range given in Ref. [41] and others ($\Delta m^2_{21} \sim 4 \times 10^{-5}\,\mathrm{eV}^2 - 3 \times 10^{-4}\,\mathrm{eV}^2$). The arrows/lines correspond to the LMA best-fit value. Figure from Ref. [35].

the determination of the neutrino mass hierarchy. Third, the observation of non-zero *CP* violation in the lepton sector if the underlying δ corresponds to maximal *CP* violation. The three groups of bars correspond to three different experimental scenarios, with different baselines. The favored scenario is the one illustrated by the bottom group of three bars, for which there are two detectors, one at $L = 7500$ km and the other at $L = 3000$ km. Note that:

At a Neutrino Factory $\sin^2 2\theta_{13}$ can be measured, the neutrino mass hierarchy determined, and a search for *CP* violation in the lepton sector made for all values of $\sin^2 2\theta_{13}$ down to $O(10^{-4})$, or even a little less.

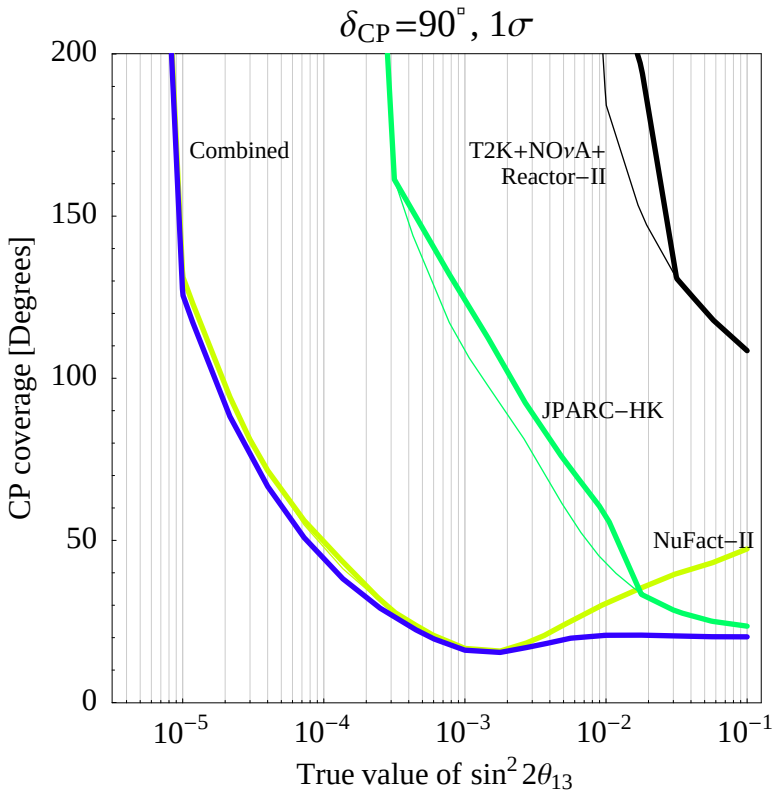

FIG. 20: (Color) The 1σ precision on the determination of the phase δ at a Neutrino Factory, and at a representative high-performance Superbeam, together with the combined Neutrino Factory plus Superbeam sensitivity. The sensitivities are shown as a function of the underlying value of $\sin^2 2\theta_{13}$. The thin curves correspond to cases where the the *sign-degeneracy* is not taken into account. Calculation from the authors of Ref. [36].

If $\sin^2 2\theta_{13}$ is fairly large, Superbeam experiments may also establish its value, and perhaps determine the mass hierarchy and begin the search for *CP* violation. Figure 20 illustrates the role of a Neutrino Factory over a broad range of $\sin^2 2\theta_{13}$ values. The figure shows, as a function of the underlying value of $\sin^2 2\theta_{13}$, the 1σ precision on the determination of the phase δ at a Neutrino Factory, and at a representative high-performance Superbeam, together with the combined Neutrino Factory plus Superbeam sensitivity. Below values of $\sin^2 2\theta_{13} \sim 10^{-2}$ the Neutrino Factory sensitivity is significantly better than the sensitivity that can be achieved with Superbeams, and indeed provides the only sensitivity to the *CP* phase if $\sin^2 2\theta_{13}$ is significantly smaller than 10^{-2}. Above $\sin^2 2\theta_{13} \sim 10^{-2}$ the Neutrino Factory measurements still enable a modest improvement to the *CP* violation measurement sensitivity, but the exact impact that a Neutrino Factory might have in this case is less

clear. The uncertainty on the matter density, which is believed to be $O(5\%)$, is likely to be a limiting uncertainty for *CP* violation measurements [42]. Improved knowledge of the matter density along the neutrino flight-path would improve the expected Neutrino Factory sensitivity. In addition, Bueno *et al.* [39] have shown that the energy dependencies of matter and *CP* violating effects are different, and can be exploited to further separate the two effects. For $\sin^2 2\theta_{13} > 0.01$, the case for a Neutrino Factory will depend upon just how well Superbeam experiments will ultimately be able to do, whether any new discoveries are made along the way that complicate the analysis, whether any theoretical progress is made along the way that leads to an emphasis on the type of measurements that a Neutrino Factory excels at, how important further tests of the oscillation formalism is in general, and the importance of observing and measuring $\nu_e \to \nu_\tau$ oscillations in particular.

We conclude there is a strong physics case for a Neutrino Factory if $\sin^2 2\theta_{13}$ **is less than** ~ 0.01**. There may also be a strong case if** $\sin^2 2\theta_{13}$ **is larger than this, but it is too early to tell.**

4. Special Case: $\theta_{13} = 0$

The case $\theta_{13} = 0$ is very special. The number of mixing angles needed to describe the 3×3 unitary neutrino mixing matrix would be reduced from three to two, suggesting the existence of a new conservation law resulting in an additional constraint on the elements of the mixing matrix. The discovery of a new conservation law happens rarely in physics, and almost always leads to revolutionary insights in our understanding of how the physical universe works. Hence, if it were possible to establish that $\theta_{13} = 0$, it would be a major discovery. Note that in the limit $\theta_{13} \to 0$, the oscillation probability for $\nu_e \leftrightarrow \nu_\mu$ transitions is finite, and is given by:

$$P\left(\nu_e \to \nu_\mu\right) \;=\; \frac{\Delta m^2_{21}}{\Delta m^2_{31}} \sin^2 2\theta_{12} \cos^2 \theta_{23} \frac{\sin^2 A\Delta}{A^2}\,, \tag{7}$$

where the matter parameter $A = 1$ if the neutrino energy corresponds to the matter resonance, which for a long-baseline terrestrial experiment means neutrino energies $E \sim 12$ GeV. In addition, if the baseline L is chosen such that L/E corresponds to the oscillation maximum, then $\sin^2 \Delta = 1$, and we have that

$$P(\nu_e \to \nu_\mu) \sim \sin^2 2\theta_{12} \cos^2 \theta_{23} \frac{\Delta m^2_{21}}{\Delta m^2_{31}}. \tag{8}$$

Substituting into this expression values for the oscillation parameters that are consistent with the present solar and atmospheric neutrino data, we are led to conclude that even if $\theta_{13} = 0$, provided the neutrino energy and baseline are chosen appropriately, $\nu_e \leftrightarrow \nu_\mu$ transitions are still directly observable in an appearance experiment if oscillation probabilities of $O(10^{-4})$ are observable. Hence, if θ_{13} is very small, the ideal neutrino oscillation experiment will be a long baseline experiment that uses neutrinos with energies close to 12 GeV, i.e., uses a baseline such that L/E corresponds to the oscillation maximum, and is sensitive to values of $P(\nu_e \leftrightarrow \nu_\mu) \sim 10^{-4}$ or smaller. Neutrino Factories provide the only way we know to satisfy these experimental requirements.

If $\theta_{13} = 0$ a Neutrino Factory experiment would enable (i) the first observation of $\nu_e \leftrightarrow \nu_\mu$ transitions in an appearance experiment, and (ii) an upper limit on $\sin^2 2\theta_{13}$ of $O(10^{-4})$ or smaller.

These are major experimental results that would simultaneously provide a final confirmation the three-flavor mixing framework (by establishing $\nu_e \leftrightarrow \nu_\mu$ transitions in an appearance experiment) while strongly suggesting the existence of a new conservation law. In considering the case $\theta_{13} = 0$, it should be noted that within the framework of GUT theories, radiative corrections will change the value of $\sin^2 2\theta_{13}$ measured in the laboratory from the underlying value of $\sin^2 2\theta_{13}$ at the GUT scale. Recent calculations [43] have suggested that these radiative corrections to $\sin^2 2\theta_{13}$ will be $O(10^{-4})$. If this is the case, the ultimate Neutrino Factory experiment would not only provide the first direct observation of $\nu_e \rightarrow \nu_\mu$ transitions, but would also

- establish a finite value for θ_{13} at laboratory scales consistent with being zero at the GUT scale,
- determine the sign of Δm^2_{31}, and hence determine whether the neutrino mass hierarchy is normal or inverted, and
- detect maximal CP violation in the lepton sector.

These would be tremendously important results.

V. PROGRESS ON FACILITY DESIGN

In this Section we summarize the technical work accomplished as part of the APS Study [1]; for details see a recent publication [44]. Our focus was to update the FS2 design with some of the more cost-effective approaches we have studied. In particular, a more optimized capture section was designed, a shorter and less expensive bunching and phase rotation scheme was developed, and a more optimized acceleration scheme based on a combination of RLA and FFAG rings was worked out.

A. Front End

The front end of the neutrino factory (the part of the facility between the target and the first linear accelerator) represented a large fraction of the total facility costs in FS2 [9]. However, several recent developments have given credit to the idea that a new design for the front end may be possible that is significantly less expensive:

- A new approach to bunching and phase rotation using the concept of adiabatic rf bunching [45, 46, 47, 48, 49] eliminates the very expensive induction linacs used in FS2.
- For a moderate cost, the transverse acceptance of the accelerator chain could be doubled from its FS2 value.
- This diminished the demands on the transverse ionization cooling section and allowed the design of a simplified cooling section with fewer components and reduced magnetic field strength.

We denote as *Study 2B* (S2B) the simulations that have been made of the performance of this new front end, together with the new scheme for acceleration. The Monte Carlo simulations were performed with the code ICOOL [50].

The overall layout of the new front–end design is shown in Fig. 21. The first ≈12 m is used to capture pions produced in the target. The field here drops adiabatically from 20 T over the target down to 1.75 T. At the same time, the radial aperture of the beam pipe increases from 7.5 cm at the target up to 25 cm. Next comes ≈100 m for the pions to decay into muons and for the energy-time correlation to develop. The adiabatic bunching occupies the next ≈50 m

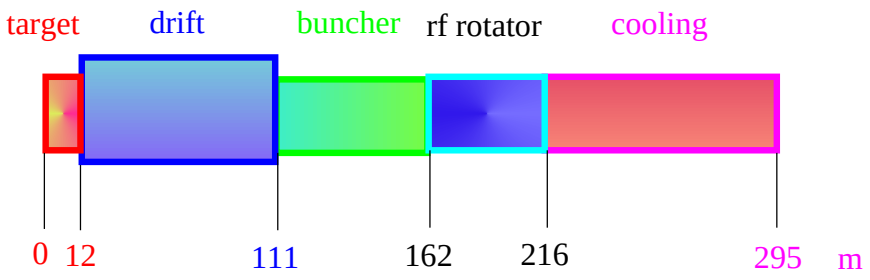

FIG. 21: (Color) Overall layout of the front-end.

and consists of 27 cavities with 13 different and decreasing frequencies (333 f 234 MHz) and a changing but increasing gradients (5 $Grad.$ 10 MV/m). This is followed by the phase rotation of ≈50 m in length and composed of 72 cavities with 15 different and decreasing frequencies (232 f 201 MHz), but constant gradient ($Grad = 12.5$ MV/m) for this section. Lastly, the channel has ≈80 m of ionization cooling. The cooling channel was designed to have a relatively flat transverse beta function with a magnitude of about 80 cm. Most of the 150 cm cell length is taken up by the 50-cm-long rf cavities. The cavities have a frequency of 201.25 MHz and a gradient of 15.25 MV/m. A novel aspect of this design comes from using the windows on the rf cavity as the cooling absorbers. This is possible because the near constant β function does not significantly increase the emittance heating at the window location. The window consists of a 1 cm thickness of LiH with 25 μm thick Be coatings (The Be will, in turn, have a thin coating of TiN to prevent multipactoring [51].) The alternating 2.8 T solenoidal field is produced with one solenoid per half cell, located between the rf cavities. The total length of the new front end is 295 m.

The reduction in normalized transverse emittance along the cooling channel is shown in the left plot of Fig. 22 and the right plot shows the normalized longitudinal emittance. The channel produces a final value of $\epsilon_T = 7.1$ mm rad, that is, more than a factor of two reduction from the initial value. The number of muons per proton that fit into the accelerator transverse normalized acceptance of $A_T = 30$ mm rad and normalized longitudinal acceptance of $A_L = 150$ mm is 0.170 ± 0.006. The 80-m-long cooling channel raises this quantity by about a factor of 1.7. This is the same value obtained in FS2. Thus, we have achieved the identical performance at the entrance to the accelerator as FS2, but with a significantly simpler, shorter, and presumably less expensive channel design. In addition, unlike FS2, this channel transmits both signs of muons produced at the target. With ap-

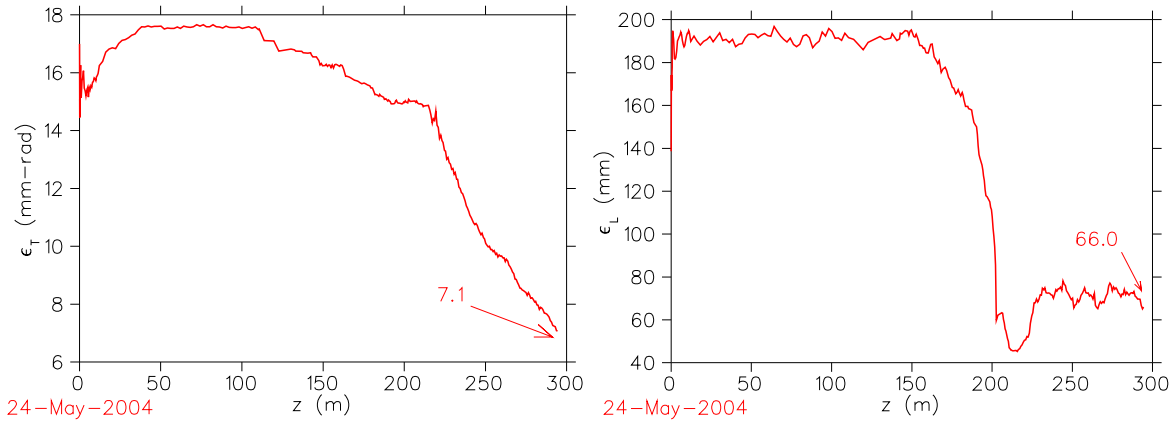

FIG. 22: (Color) Normalized transverse emittance (left) and longitudinal emittance (right) along the front-end for a momentum cut $0.1 \leq p \leq 0.3$ GeV/c.

TABLE VII: Performance of the Front-End

$< p_z >$ Mean Momentum (MeV/c)	220
rms Energy Spread (MeV)	31
(mm-rad)	7.1
$^{equil.}$(mm-rad)	5.5
$_L$(mm)	66
A (mm-rad)	30
A_L (mm)	150
No. $/p$ in A and A_L	0.176

propriate modifications to the transport line going into the storage ring, this design could deliver both (time tagged) neutrinos and antineutrinos to the detector. The performance of the front-end is summarized in Table VII

B. Acceleration

A new acceleration has been designed [44] with particular emphasis on reducing the acceleration costs in FS2. A matching section, using normal conducting rf cavities, matches the cooling channel optics to the requirements of a superconducting rf linac. This linac uses solenoidal focusing and raises the energy of the muon beam from 0.27 to 1.50 GeV. The

linac contains three parts. The cell lengths have been reduced compared to FS2 in order to increase the acceptance. The first part has only a single-cell 201 MHz cavity per period. The second part, with longer period, has a 2-cell rf cavity unit per period. The third part, as a still longer period becomes possible, accommodates two 2-cell cavity units per period. Figure 3 shows the three cryomodule types that make up the pre-accelerator linac.

The superconducting rf linac is followed by a 3.5-pass dogbone RLA, shown in Fig. 4, that raises the energy from 1.5 to 5 GeV. For a given amount of installed rf, the dogbone layout has twice the energy separation of a racetrack configuration, making the switchyard design easier and allowing more passes through the RLA linac. This RLA uses four 2-cell superconducting rf cavity structures per cell, and utilizes quadrupole triplet (as opposed to solenoidal) focusing. The RLA has just over 1 GeV of installed linac. Acceleration to 5 GeV takes $3\frac{1}{2}$ passes.

Following the RLA are two cascaded FFAG rings that increase the beam energy from 5 to 10 GeV, and 10 to 20 GeV, respectively. Each ring uses combined-function magnets arranged in a doublet focusing arrangement. The lower energy FFAG ring has a circumference of about 286 m; the higher energy ring is about 400 m in circumference. Tracking studies showed that the longitudinal dynamics in the FFAGs were well understood.

An effort was made to achieve a reasonably cost-optimized design. Without detailed engineering, it is not possible to fully optimize costs, but we have employed general formulae that properly represent the cost trends and that were considered adequate to make choices at the present stage of the design. As the acceleration system was one of the dominant cost items in FS2, we are confident that the approach adopted here will result in a less expensive Neutrino Factory facility with essentially the same performance as calculated for the FS2 design.

VI. NEUTRINO FACTORY R&D

As should be clear from the design descriptions in Section V, the muon-based Neutrino Factory is a demanding project. This type of machine make use of novel components and techniques that are, in some cases, at or beyond the state of the art. For this reason, it is critical that R&D efforts to study these matters be carried out. In this Section we describe the main areas of R&D effort under way in support of the project. We give an overview of

the R&D program goals and list the specific questions we expect ultimately to answer. We also summarize briefly the R&D accomplishments to date and give an indication of R&D plans for the future.

Since the Neutrino Factory is not expected to begin construction in the near future, it might be asked why it is necessary to pursue a vigorous R&D program now. One answer is that this R&D is what allows us to determine—with some confidence—both the expected performance and expected cost of such machine. This information must be available in a timely way to permit the scientific community to make informed choices on which project(s) they wish to request at some future time. Experience has shown that large, complex accelerator projects take many years of preparatory R&D in advance of construction. It is only by supporting this R&D effort now that we can be ready to provide a Neutrino Factory when the proper time comes.

A. Neutrino Factory R&D

Successful construction of a muon storage ring to provide a copious source of neutrinos requires many novel approaches to be developed and demonstrated; a high-luminosity Muon Collider, which might someday follow, would require an even greater extension of the present state of accelerator design. Thus, reaching the desired facility performance requires an extensive R&D program. Each of the major systems has significant issues that must be addressed by R&D activities. Component specifications need to be verified. For example, the cooling channel assumes a normal conducting rf (NCRF) cavity gradient of 15 MV/m at 201.25 MHz, and the acceleration section demands similar performance from superconducting rf (SCRF) cavities at the same frequency. In both cases, the requirements are beyond the performance reached to date for cavities in this frequency range. The ability of the target to withstand a proton beam power of up to 4 MW must be confirmed. Finally, an ionization cooling experiment should be undertaken to validate the implementation and performance of the cooling channel, and to confirm that our simulations of the cooling process are accurate.

1. R&D Program Overview

A Neutrino Factory comprises the following major systems: Proton Driver; Target, (Pion) Capture, and (Pion-to-Muon) Decay Section; Bunching and Phase Rotation Section; Cooling Section; Acceleration Section; and Storage Ring (Muon-to-Neutrino). The R&D program we envision is designed to answer first the key questions needed to embark upon a Zeroth-order Design Report (ZDR). The ZDR will examine the complete systems of a Neutrino Factory, making sure that nothing is forgotten, and will show how the parts merge into a coherent whole. While it will not present a fully engineered design with a detailed cost estimate, enough detail will be presented to ensure that the critical items are technically feasible and that the proposed facility could be successfully constructed and operated at its design specifications. By the end of the full R&D program, it is expected that a formal Conceptual Design Report (CDR) for a Neutrino Factory could begin. The CDR would document a complete and fully engineered design for the facility, including a detailed bottom-up cost estimate for all components. This document would form the basis for a full technical, cost, and schedule review of the construction proposal, subsequent to which construction could commence (assuming strong community support and government approval). The R&D issues for each of the major systems must be addressed by a mix of theoretical, simulation, modeling, and experimental studies, as appropriate. A list of the key physics and technology issues for each major Neutrino Factory system is given below. These issues are being actively pursued as part of the ongoing worldwide Neutrino Factory R&D program, with participation from Europe, Japan, and the U.S.

Proton Driver

- Production of intense, short proton bunches, e.g., with space-charge compensation and/or high-gradient, low frequency rf systems

Target, Capture, and Decay Section

- Optimization of target material (low-Z or high-Z) and form (solid, moving band, liquid-metal jet)
- Design and performance of a high-field solenoid ($\approx$20 T) in a very high radiation environment

Bunching and Phase Rotation Section

- Design of efficient and cost-effective bunching system
- Examination of alternative approaches, e.g., based upon combined rf phase rotation and bunching systems or fixed-field, alternating gradient (FFAG) rings

Cooling Section

- Development and testing of high-gradient normal conducting rf (NCRF) cavities at a frequency near 200 MHz
- Development and testing of efficient high-power rf sources at a frequency near 200 MHz
- Development and testing of LH_2, LiH, and other absorbers for muon cooling
- Development and testing of candidate diagnostics to measure emittance and optimize cooling channel performance

Acceleration Section

- Optimization of acceleration techniques to increase the energy of a muon beam (with a large momentum spread) from a few GeV to a few tens of GeV (e.g., recirculating linacs, rapid cycling synchrotrons [52], FFAG rings)
- Development of high-gradient superconducting rf (SCRF) cavities at frequencies near 200 MHz, along with efficient power sources (about 10 MW peak) to drive them
- Design and testing of components (rf cavities, magnets, diagnostics) that will operate in the muon-decay radiation environment

Storage Ring

- Design of large-aperture, well-shielded superconducting magnets that will operate in the muon-decay radiation environment

2. Recent R&D Accomplishments

a. Targetry The BNL Targetry experiment, E951, has carried out initial beam tests [53] of both a solid carbon target and a mercury target at a proton beam intensity of about 4×10^{12} ppp. In the case of the solid carbon target, it was found that a carbon-carbon composite having nearly zero coefficient of thermal expansion is largely immune to beam-induced pressure waves. A carbon target in a helium atmosphere is expected to have negligible sublimation loss. A program to verify this is under way at ORNL [54]. If radiation damage is the limiting effect for a carbon target, the predicted lifetime would be about 12 weeks when bombarded with a 1 MW proton beam.

For a mercury jet target, tests with about 2×10^{12} ppp showed that the jet is not dispersed until long after the beam pulse has passed through the target (see Fig. 23). Measurements of the velocity of droplets emanating from the jet as it is hit by the proton beam pulse from the AGS ($\approx$10 m/s for 25 J/g energy deposition) compare favorably with simulation estimates. High-speed photographs indicate that the beam disruption at the present intensity does not propagate back upstream toward the jet nozzle. If this remains true at the higher intensity of 1.6×10^{13} ppp, it will ease mechanical design issues for the nozzle.

FIG. 23: Disruption of Hg jet hit with AGS beam bunch containing 2×10^{12} protons. Frames from left to right correspond to time steps of 0, 0.75, 2, 7, and 18 ms, respectively.

b. MUCOOL A primary effort has been to carry out high-power tests of 805-MHz rf cavities in the Lab G test area at Fermilab. A 5-T test solenoid for the facility, capable of operating either in solenoid mode (its two independent coils powered in the same polarity) or gradient mode (with the two coils opposed), was used to study the effects of magnetic field on cavity performance. Most recently, a single-cell 805-MHz pillbox cavity (Fig. 24) having Be foils to close the beam iris was tested. This cavity permitted an assessment of the behavior of the foils under rf heating and was used to study dark current effects [55]. The

cavity reached 40 MV/m (exceeding its design specification) in the absence of a magnetic field, but was limited by breakdown to less than 15 MV/m at high magnetic field ($\approx$ 2 T). Understanding the effects of the magnetic field on cavity performance is crucial, as this is the environment required for cavities in a muon cooling channel.

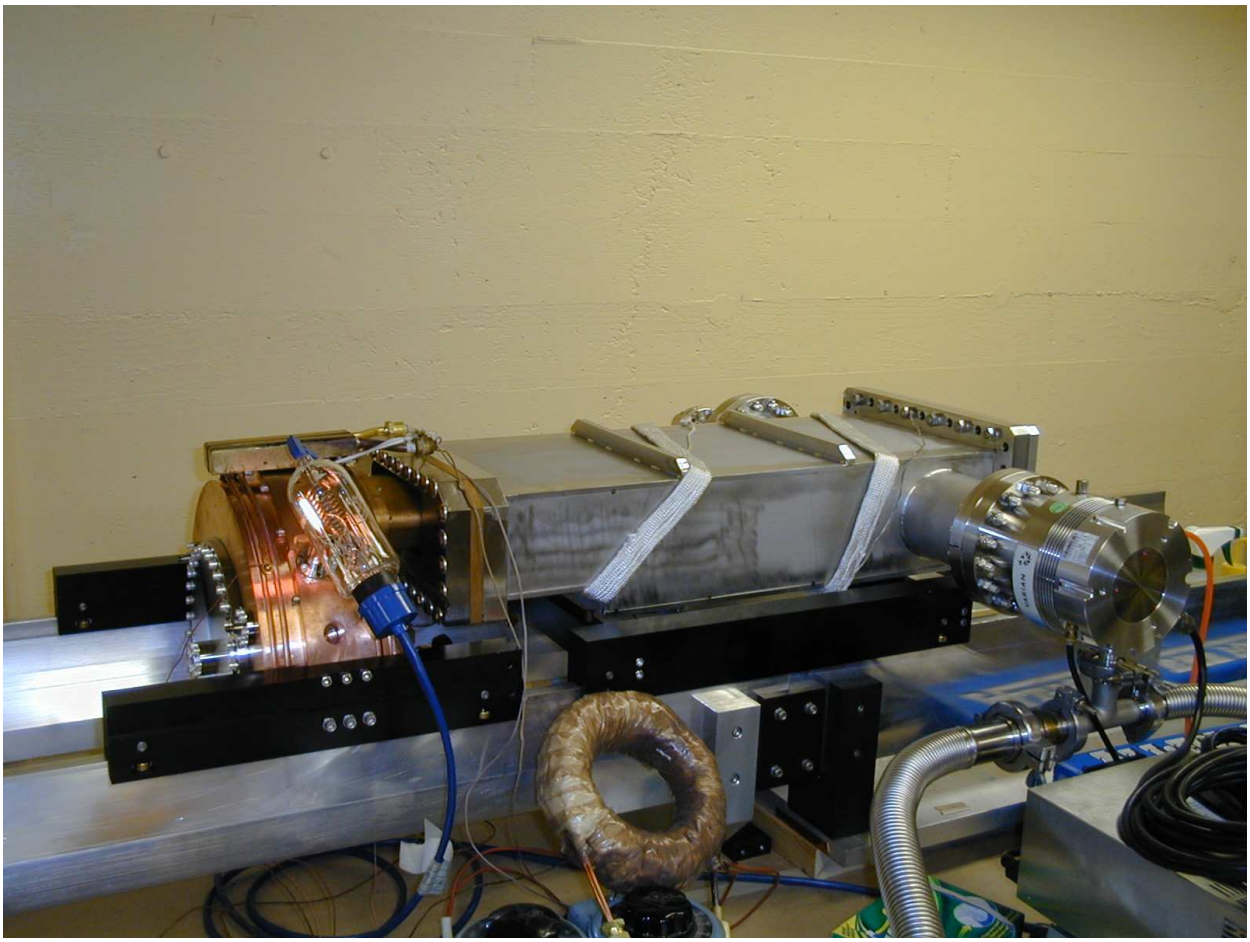

FIG. 24: (Color) 805 MHz pillbox rf cavity used for testing. The cavity has removable windows to permit tests of different window materials, and a thin exit port to permit dark current studies.

Development of a prototype LH_2 absorber, the material chosen for FS2 and also for MICE [56] (the Muon Ionization Cooling Experiment, see Section VI A 4) is well along. Several large diameter, thin (125–350 μm) aluminum windows have been successfully fabricated by machining from solid disks. These have been pressure tested with water and found to break at a pressure consistent with finite-element design calculations [57]. Another absorber material that must be studied is LiH, the material on which the cooling channel used in this report is based. In the new scheme, the LiH serves both as an absorber and an rf window.

This configuration could be tested in the 805-MHz pillbox cavity described above. A new area, the MUCOOL Test Area (MTA), is nearly completed at FNAL and will be used for initial testing of the liquid-hydrogen absorbers. It will also have access to both 805-MHz and 201-MHz high-power rf amplifiers for continuing rf tests of the 805-MHz pillbox cavity and, soon, for testing a prototype 201-MHz cavity. The MTA is located at the end of the Fermilab proton linac, and is designed to eventually permit beam tests of components and detectors with 400 MeV protons.

c. Beam Simulations and Theory Subsequent to work on FS2, present effort has focused on further optimization of Neutrino Factory performance and costs. The more cost effective front-end design reported in this paper is a result of this work.

d. SCRF Development This work is aimed at development of a high-gradient 201-MHz SCRF cavity for muon acceleration. (The choice of SCRF for a cooling channel is excluded because of the surrounding high magnetic field; the acceleration system does not suffer this limitation.) A test area of suitable dimensions was constructed at Cornell (Fig. 25) and used to test a prototype cavity fabricated for the Cornell group by CERN colleagues. The cavity reached 11 MV/m in initial tests, but exhibited a significant "Q slope" as the gradient increased [58]. To better understand the origins of this phenomenon, effort will shift to studies on a smaller 500 MHz cavity. Different coating and cleaning techniques will be explored to learn how to mitigate the observed Q slope.

FIG. 25: (Color) 201 MHz SCRF cavity being prepared for testing at Cornell.

3. R&D plans

a. Targetry For the targetry experiment, design of a pulsed solenoid and its power supply are under way. A cost-effective design capable of providing up to a 15 T field has been developed (see Fig. 26). Tests of a higher velocity mercury jet (about 20 m/s velocity,

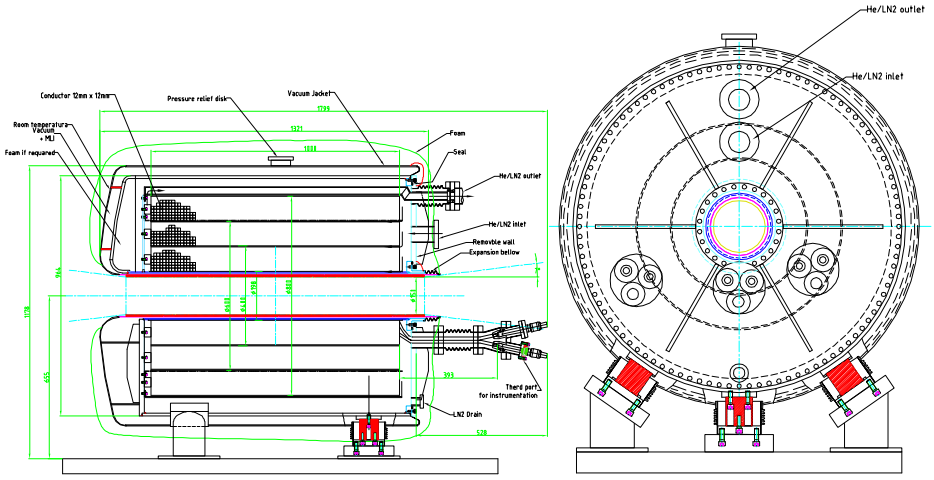

FIG. 26: (Color) Design of targetry test magnet. The magnet has three nested coils that permit operation at 5, 10, and 15 T. The coils are normal conducting but cooled to liquid-nitrogen temperature to ease the requirements on the power supply.

compared with about 2.5 m/s in the jet system initially tested), will be carried out. To complement the experimental program, target simulation efforts are ongoing. These aim at a sufficiently detailed understanding of the processes involved to reproduce the observed experimental results both with and without a magnetic field. Fully 3D magneto-hydrodynamics codes are being utilized for this effort.

b. MUCOOL Further testing work for 805 MHz components will continue in the MTA. Work will focus on understanding and mitigating dark current and breakdown effects at high gradient. Many aspects of cavity design, such as cleaning and coating techniques, will be investigated. In addition, tests of alternative designs for window or grid electromagnetic terminations for the rf cavity will be initially explored to identify the best candidates for the full-sized 201 MHz prototype cavity. Fabrication of the 201 MHz cavity by a group from LBNL, Jlab, and the University of Mississippi is nearly completed. This cavity will also be tested in the MTA. Thermal tests of a prototype absorber in the MTA are just getting under way. Fabrication of other cooling channel components required for the initial phase of

testing will be carried out, including a large-bore superconducting solenoid, and diagnostics that could be used for the experiment. With these components, it will be possible eventually to assemble and bench test a full prototype cell of a realistic cooling channel. Provision will be made to test curved Be windows and grids in the 805 MHz cavity, followed by tests on the 201 MHz prototype. As already noted, the site of the MTA was selected with the goal of permitting beam tests of the cooling channel components with a high intensity beam of 400 MeV protons. While not the same as using an intense muon beam, such a test would permit a much better understanding of how the cooling channel would perform operationally, especially the high-gradient rf cavity and the LH_2 or LiH absorber.

c. Beam Simulations and Theory A major simulation effort will continue to focus on iterating the front-end channel design to optimize it for cost and performance. Further effort will be given to beam dynamics studies in the FFAG rings and storage ring, including realistic errors. Work on optimizing the optics design will be done. Assessment of field-error effects on the beam transport will be made to define acceptance criteria for the magnets. This will require use of sophisticated tracking codes, such as COSY [59], that permit rigorous treatment of field errors and fringe-field effects. In many ways, the storage ring is one of the most straightforward portions of a Neutrino Factory complex. However, beam dynamics is an issue here as the muon beam must circulate for many hundreds of turns. Use of a tracking code such as COSY is required to assess fringe field and large aperture effects. As with the FFAG rings, the relatively large emittance and large energy spread enhance the sensitivity to magnetic field and magnet placement errors. Suitable magnet designs are needed, with the main technical issue being the relatively high radiation environment. Another lattice issue that must be studied is polarization measurement. In the initial implementation of a Neutrino Factory it is expected that polarization will not be considered, but its residual value may nonetheless be important in analyzing the experiment. Simulation efforts in support of MICE will continue. We also plan to participate in a so-called "World Design Study" of an optimized Neutrino Factory. This study, an international version of the two previous U.S. Feasibility Studies, will likely be hosted in the UK by Rutherford Appleton Laboratory (RAL), the site for the MICE experiment (see Section VI A 4). It will be organized jointly by representatives from Europe, Japan, and the U.S.

d. SCRF Development A prototype 500 MHz SCRF cavity will be used to study the Q slope phenomenon, with the goal of developing coating and cleaning techniques that

reduce or eliminate it. Detuning issues at 201 MHz associated with the very large cavity dimensions and the pulsed rf system will be evaluated. Tests of the 201 MHz SCRF cavity will include operation in the vicinity of a shielded solenoid magnet, to demonstrate our ability to adequately reduce nearby magnetic fields in a realistic lattice configuration. If funds permit, design of a prototype high-power rf source will be explored, in collaboration with industry. This source—presently envisioned to be a multibeam klystron—must be developed for operation at two different duty factors, because the cooling channel requires a duty factor of about 0.002 whereas the acceleration chain requires 0.045. Magnet designs suitable for the FFAG rings and the muon storage ring will be examined further. Both conventional and superconducting designs will be compared where both are possible. With SC magnets, radiation heating becomes an issue and must be assessed and dealt with.

4. Cooling Demonstration Experiment

Clearly, one of the most important R&D tasks that is needed to validate the design of a Neutrino Factory is to measure the cooling effects of the hardware we propose. Participation in the International Muon Ionization Cooling Experiment (MICE) will accomplish this, and is therefore expected eventually to grow into a primary activity. Unquestionably, the experience gained from this experiment will be invaluable for the design of an actual cooling channel.

At the NUFACT'01 Workshop in Japan, a volunteer organization was created to organize a cooling demonstration experiment that might begin as soon as 2004. Membership in this group includes representatives from Europe, Japan, and the U.S. The experimental collaboration now numbers some 140 members from the three geographical regions. The MICE Collaboration has received scientific approval for the experiment from RAL management, and is now in the process of seeking funding. The experiment will involve measuring, on a particle-by-particle basis, the emittance reduction produced by a single cell of the FS2 cooling channel. A schematic of the layout is shown in Fig. 27. The cooling channel cell is preceded and followed by nearly identical detector modules that accomplish particle identification and emittance measurement. Provision for testing a series of absorber materials, including both LH_2 and solid absorbers, has been made. A preliminary safety review of the liquid-hydrogen system has been successfully passed, and permission to begin detailed

engineering has been granted.

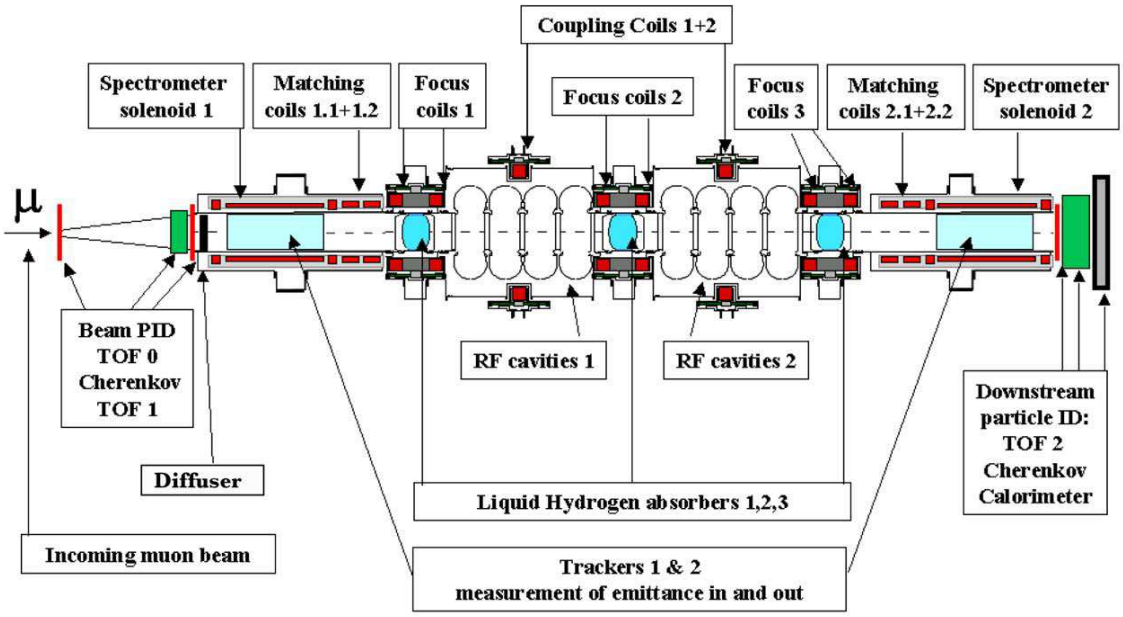

FIG. 27: (Color) Schematic of the MICE layout.

VII. SUMMARY

A new type of facility have been proposed that could have a tremendous impact on future neutrino experiments—the Neutrino Factory. In contrast to conventional muon-neutrino beams, Neutrino Factory would provide a source of electron-neutrinos (ν_e) and -antineutrinos ($\bar{\nu}_e$), with very low systematic uncertainties on the associated beam fluxes and spectra. The experimental signature for $\nu_e \rightarrow \nu_\mu$ transitions is extremely clean, with very low background rates. Hence, Neutrino Factories would enable very sensitive oscillation measurements to be made. This is so because such facility not only provides very intense beams at high energy, but also provides muon-neutrinos (ν_μ) and -antineutrinos ($\bar{\nu}_\mu$) in addition to electron-neutrinos (ν_e) and -antineutrinos ($\bar{\nu}_e$). This would facilitate a large variety of complementary oscillation measurements in a single detector, and dramatically improve our ability to test the three-flavor mixing framework, measure *CP* violation in the lepton sector (and perhaps determine the neutrino mass hierarchy), and, if necessary, probe extremely small values of the mixing angle θ_{13}.

At this time, we do not know the value of θ_{13}. If $\sin^2 2\theta_{13} < 0.01$, much of the ba-

sic neutrino oscillation physics program will be beyond the reach of conventional neutrino beams. In this case Neutrino Factories offer the only known way to pursue the desired physics program.

An impressive Neutrino Factory R&D effort has been ongoing in the U.S. and elsewhere over the last few years, and significant progress has been made towards optimizing the design, developing and testing the required accelerator components, and significantly reducing the cost, even during the current Study. (Although a full engineering study is required, we have preliminary indications that the unloaded cost of a Neutrino Factory facility based on an existing Superbeam proton driver and target station can be reduced substantially compared with previous estimates.) Neutrino Factory R&D has reached a critical stage in which support is required for two key international experiments (MICE and Targetry) and a third-generation international design study. If this support is forthcoming, a Neutrino Factory could be added to the Neutrino Physics roadmap in about a decade.

Given the present uncertainty about the size of θ_{13}, *it is critical to support an ongoing and increased U.S. investment in Neutrino Factory accelerator R&D to maintain this technical option.* A Neutrino Factory cannot be built without continued and increased support for its development. We note that the 2001 HEPAP Report advocated an annual U.S. investment of \$8M on Neutrino Factory R&D. The present support is much less than this. Since R&D on the design of frontier accelerator facilities takes many years, support must be provided *now* to have an impact in about a decade.

Acknowledgments

This research was supported by the U.S. Department of Energy under Contracts No. DE-AC02-98CH10886, No. DE-AC02-76CH03000, and No. DE-AC03-76SF00098.

---

[1] *APS Multi-Divisional Study of the Physics of Neutrinos*, `http://www.aps.org/neutrino/`, sponsored by the American Physical Society Divisions of: Nuclear Physics, Particles and Fields, Astrophysics, Physics of Beams (2004).

[2] S. Geer, Phys. Rev. **D57**, 6989 (1998), *ibid.* **59**, 039903E (1999).

[3] M. M. Alsharo´a *et al.*, Phys. Rev. ST Accel. Beams **6**, 081001 (2003).

[4] A. Blondel *et al.*, CERN 2004-002 ECFA/CERN.

[5] The Neutrino Factory and Muon Collider Collaboration WEB page, `http://www.cap.bnl.gov/mumu/`.

[6] `http://hepunx.rl.ac.uk/neutrino-factory/`.

[7] `http://muonstoragerings.web.cern.ch/muonstoragerings/`.

[8] `http://www-prism.kek.jp/nufactj/index.html`.

[9] S. Ozaki, R. Palmer, M. Zisman, and J. Gallardo, eds., Tech. Rep., BNL-52623 (2001), `http://www.cap.bnl.gov/mumu/studyii/FS2-report.html`.

[10] N. Holtkamp and D. Finley, eds., Tech. Rep. Fermilab-Pub-00/108-E, Fermilab (2000), `http://www.fnal.gov/projects/muon_collider/nu-factory/nu-factory.html`.

[11] *The Proton Driver Design Study*, FERMILAB-TM-2136 (2000).

[12] *Proton Driver Study II*, FERMILAB-TM-2169 (Parts I and II) (2002).

[13] N. Mokhov, in *Proceedings of the 2001 Particle Accelerator Conference* (2001), p. 745, see also `http://www-ap.fnal.gov/MARS/`.

[14] J.R. Miller *et al.*, IEEE Trans. Magn. **30**, 1563 (1994).

[15] N. Mokhov, `http://www-ap.fnal.gov/MARS/`, nucl-th/9812038.

[16] T. Gaisser, *Cosmic Rays and Particle Physics* (Cambridge University Press, 1990).

[17] D. MacFarlane *et al.* (CCFR), Z. Phys. **C26**, 1 (1984), J.P. Berge *et al.* (CDHSW), Z. Phys. **C35**, 443 (1987), J.V. Allaby *et al.* (CHARM), Z. Phys. **C38**, 403 (1988), P. Auchincloss *et al.* (E701), Z. Phys. **C48**, 411 (1990), world average from J. Conrad, M. Shaevitz and T. Bolton, Rev. Mod. Phys. **70**, 1341 (1998).

[18] *MINOS Technical Design Report*, `http://www.hep.anl.gov/ndk/hypertext/minos_tdr.html` , nuMI-L-337 TDR.

[19] V. Barger, S. Geer and K. Whisnant, Phys. Rev. **D61**, 053004 (2000), hep-ph/9906487.

[20] C. Crisan and S. Geer, Tech. Rep., FERMILAB-TM-2101 (2000).

[21] A. De Rujula, M. B. Gavela and P. Hernandez, Nucl. Phys. **B547**, 21 (1999), hep-ph/9811390.

[22] A. Cervera, A. Donini, M. B. Gavela, J. J. Gomez Cadenas, P. Hernandez, O. Mena and S. Rigolin, Nucl. Phys. **B579**, 17 (2000), hep-ph/0002108. Erratum: ibid. **B593**, 731 (2001).

[23] C. Albright, *et al.*, Tech. Rep., Fermilab (2000), report to the Fermilab Director; Fermilab-FN-692, May 10; hep-ex/0008064.

[24] M. Apollonio *et al.* (CERN working group on oscillation physics at the Neutrino Factory),

Oscillation physics with a neutrino factory (2002), hep-ph/0210192.

[25] S. Geer, Comments Nucl. Part. Phys. **A2**, 284 (2002), hep-ph/0008155.

[26] V. Barger, S. Geer, R. Raja, and K. Whisnant, Phys. Rev. **D63**, 033002 (2000).

[27] V. Barger, S. Geer, R. Raja, and K. Whisnant, Phys.Rev. **D63**, 113011 (2000).

[28] H. Minakata and H. Nunokawa, JHEP **10**, 001 (2001), hep-ph/0108085.

[29] W. Winter, Phys. Rev. **D70**, 033006 (2004), hep-ph/0310307.

[30] G. L. Fogli and E. Lisi, Phys. Rev. **D54**, 3667 (1996), hep-ph/9604415.

[31] J. Burguet-Castell, M. B. Gavela, J. J. Gomez-Cadenas, P. Hernandez and O. Mena, Nucl. Phys. **B608**, 301 (2001), hep-ph/0103258.

[32] V. Barger, D. Marfatia and K. Whisnant, Phys. Rev. **D65**, 073023 (2002), hep-ph/0112119.

[33] J. Burguet-Castell, M. B. Gavela, J. J. Gomez-Cadenas, P. Hernandez and O. Mena, Nucl. Phys. **B646**, 301 (2002), hep-ph/0207080.

[34] A. Donini, D. Meloni and F. Migliozzi, J. Phys. **G29**, 1865 (2003), hep-ph/0209240.

[35] P. Huber and W. Winter, Phys. Rev. **D68**, 037301 (2003), hep-ph/0301257.

[36] P. Huber, M. Lindner, and W. Winter, Nucl. Phys. **B645**, 3 (2002), hep-ph/0204352.

[37] D. Autiero *et al.*, Eur. Phys. J. **C33**, 243 (2004), hep-ph/0305185.

[38] A. Donini, D. Meloni and P. Migliozzi, Nucl. Phys. **B646**, 321 (2002), hep-ph/0206034.

[39] A. Bueno, M. Campanelli, A. Rubbia, Nucl. Phys. **B589**, 577 (2000), hep-ph/0005007.

[40] P. Huber, M. Lindner and W. Winter, `http://www.ph.tum.de/~globes`.

[41] M. Maltoni, T. Schwetz and J.W.F. Valle, Phys. Rev. **D67**, 093003 (2003).

[42] T. Ohlsson and W. Winter, Phys. Rev. **D68**, 073007 (2003), hep-ph/0307178.

[43] J.A. Aguilar-Saavedra, G.C. Branco, and F.R. Joaquim, Phys. Rev. **D69**, 073004 (2004), hep-ph/0310305.

[44] J.S. Berg *et al.*, *A Cost-Effective Design for a Neutrino Factory*, submitted to Phys. Rev. ST-AB.

[45] D. Neuffer, *Exploration of the high-frequency buncher concept*, MUC-NOTE-269 (2003), all MUC-NOTE papers are available from `http://www-mucool.fnal.gov/notes/noteSelMin.html`.

[46] D. Neuffer, *Beam dynamics problems of the muon collaboration: ν-factory and $\mu^+ - \mu^-$ colliders*, MUC-NOTE-266 (2003).

[47] D. Neuffer, *High-frequency buncher and phase rotation for the muon source*, MUC-NOTE-181

(2000).

[48] D. Neuffer and A. Van Ginneken, Proceedings of the 2001 Particle Accelerator Conference (2001), http://accelconf.web.cern.ch/Accel/Conf/p01/PAPERS/TPPH162.pdf.

[49] A. Van Gineeken, Tech. Rep., Fermilab (2001), MUC-NOTE-220.

[50] R. Fernow, in *Proceedings of the 1999 Particle Accelerator Conference*, edited by A. Luccio and W. MacKay (1999), p. 3020, latest version available at http://pubweb.bnl.gov/people/fernow/icool/readme.html.

[51] A. Chao and M. Tigner, eds., *Handbook of Accelerator Physics and Engineering* (World Scientific, 1999).

[52] D.J. Summers, J.S Berg, A.A. Garren, R.B. Palmer, J. Phys. **G29**, 1727 (2003).

[53] A. Hassenein *et al.*, Nucl. Instrum. & Meth. **A503**, 70 (2003).

[54] T. Gabriel and J. Haines (2004), private communication.

[55] J. Norem, *et al.*, Phys. Rev. ST Accel. Beams **6**, 072001 (2003), also MUC-NOTE-226 (2001).

[56] R. Edgecock, J. Phys. **G29**, 1601 (2003), see also the MICE Proposal, http://mice.iit.edu/mnp/MICE0021.pdf.

[57] M.A. Cummings *et al.*, J. Phys. **G29**, 1689 (2003).

[58] R.L. Geng *et al.*, in *Proceedings of the 2003 Particle Accelerator Conference*, edited by J. Chew, P. Lucas, and S. Webber (2003), p. 1309.

[59] K. Makino and M. Berz, Nucl. Instrum. & Meth. **A427**, 338 (1999).